March, 1970

Final Report ESL-FR-418
M.I.T. DSR Project 76343
NASA Research Grant ~~NsG-234-61~~
NASA CR 110153
NGR-22-009-007

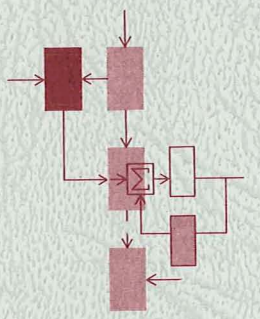

VENUS RADAR SYSTEMS INVESTIGATIONS FINAL REPORT

J. F. Reintjes
J. R. Sandison

Electronic Systems Laboratory

MASSACHUSETTS INSTITUTE OF TECHNOLOGY, CAMBRIDGE, MASSACHUSETTS 02139

Department of Electrical Engineering

March, 1970 Report ESL-FR-418

VENUS RADAR SYSTEMS INVESTIGATIONS

FINAL REPORT

by

J. F. Reintjes and J. R. Sandison

The preparation and publication of this report, including the research on which it is based, was sponsored by the National Aeronautics and Space Administration under Research Grant No. ~~NsG-234~~-61, M.I.T. DSR Project 76343. This report is published for information purposes only and does not represent recommendations or conclusions of the sponsoring agency. Reproduction in whole or in part is permitted for any purpose of the United States Government.

NGR-22-009-007

Electronic Systems Laboratory
Department of Electrical Engineering
Massachusetts Institute of Technology
Cambridge, Massachusetts 02139

ABSTRACT

This final report summarizes research activities conducted under a program entitled "Venus Radar Systems Investigations". The work was performed through grants from the National Aeronautics and Space Administration to the Electronic Systems Laboratory, Massachusetts Institute of Technology.

Initial efforts were on the design of scientific experiments for characterizing the roughnesses of planetary surfaces as determined by means of an instrument located in a spacecraft. Special attention was given to surface measurements of Planet Venus. Included in these studies were considerations of spacecraft trajectories, expected miss distances, and techniques for gathering data.

A major objective of the project was to develop instrumentation which would be capable of making the required measurements and which would meet the rigid requirements of the space environment.

A radar-type instrument that measures electromagnetic backscatter was designed and constructed; the instrument was tested while installed in a fixed-wing aircraft. The radar may be characterized as being lightweight and having low-power consumption; it is all solid-state with the exception of its low-power filament klystron transmitter. In the test program the instrument was flown in a NASA CV-990 aircraft and data on the X-band backscattering properties of various earth surfaces was determined. The results of experiments showed that gross surface features can be deduced by measurements of this kind.

A high degree of precision and repeatability in instrument performance was necessary in order to make the measurements. Thus a precise set of test and calibration procedures, in addition to specialized calibration equipment itself, was necessary.

A by-product of the work is a preliminary design for a dual-mode radar-radiometer measuring instrument which can obtain measurements of radiant energy from a surface as well as microwave electromagnetic backscatter measurements.

ACKNOWLEDGEMENT

The work described in this report has been supported as part of the Planetary Astronomy Program, Office of Space Science and Applications, National Aeronautics and Space Administration, Grants NsG-234-61 and NGR 22-009-007. The transmitter tube used in our equipment was developed under a program sponsored by the E/M Microwave Radiation Laboratory at the Electronics Research Center, NASA, Grant NAS 12-504/NASA-ERC. We wish to express our gratefulness to the personnel at NASA Headquarters for their support of the program, to the personnel at the NASA Ames Research Center who provided facilities for flight testing, and to personnel at NASA-ERC for their support of the klystron development.

CONTENTS

CONTENTS (Contd.)

LIST OF FIGURES

LIST OF FIGURES (Contd.)

I. INTRODUCTION

OBJECTIVES

A research program in microwave-pulse systems was initiated in 1961 by the National Aeronautics and Space Administration at the Electronic Systems Laboratory, M.I.T., in recognition of a need for the development of microwave electronics that are uniquely adapted to the space environment. Throughout the program emphasis was placed on the development of solid-state microwave systems and pulse circuitry that are characterized by high reliability, long life, minimum power consumption, light weight, wide operating-temperature ranges and insensitivity to external radiation sources.

In order to provide tangible design goals, the project focussed on a microwave pulse system that might be useful for exploring the surface of the planet Venus from a spacecraft. Since this planet is cloud-covered, microwaves are a logical substitute for optics in instrumentation that seeks to penetrate the cloud structure.

An additional objective of the program was to interest faculty and students in space research by providing them with opportunities to become directly involved in a space-related project.

PROGRAM SUMMARY

The program evolved under three headings:

Design of Venus surface-measurement experiments

Development of instrumentation, including necessary calibration equipment

Aircraft flight tests of an experimental instrument in an earth-bound environment

Substantial effort was placed on a study of the interrelated factors of surface roughness as interpreted from microwave-backscatter observations, plausible microwave-instrument parameters, and expected spacecraft trajectories. Trade-off studies among miss distances, radar-instrument parameters and resolvability of discrete

surface patches were made and are reported in publications of the project.[6, 8*] As a result of these studies, parameters were selected for a prototype instrument which served as a project goal.

During the early stages of the project, very little solid-state circuitry and subsystems were commercially available. A concentrated effort was therefore placed on the development of appropriate devices as in-house projects and through outside sources. In addition, since the function of the equipment was to make measurements with errors less than ±5 percent, a substantial effort was put forth on instrument stability and instrument calibration equipment. From this part of the program there evolved a capability to implement an all solid-state instrument (except for the transmitter tube) that measures transmitted and backscatter energy on a pulse-by-pulse basis.

A prototype pulse-type radar instrument that embodied the solid-state devices developed by the group was designed, constructed, and flight-tested in an aircraft. Flight testing was performed in the NASA CV-990 airborne laboratory based at Ames Research Center, Moffet Field, California. Extensive measurements of backscatter from a variety of earth surfaces were made on flights over western United States. The results of these tests show that it is possible to make some gross statements about surface roughnesses from knowledge of the magnitude of the backscatter and the profile of backscatter amplitude as a function of microwave-illumination angle.[1, 2]

On the educational side, the program offered substantial opportunities for graduate and undergraduate student participation, particularly through thesis projects. A total of eighteen theses were completed, divided as follows: 1 Doctor of Science, 10 Master of Science, and 5 Bachelor of Science. Other publications of the group include 6 technical papers, 8 technical reports, and 3 status reports.

---

* Superscripts refer to the numbered items in the list of publications at the end of the report.

II. MICROWAVE BACKSCATTER MEASUREMENTS FROM A SPACECRAFT

A. QUALITATIVE DISCUSSION

The cloud cover that envelops planet Venus prohibits straightforward observations of its surface by visual-optics means. Although the precise content of the Venusian atmosphere is still somewhat controversial, it is agreed by most investigators that a large amount of CO_2 is present. On this basis microwave radiation in the C-band, S-band and longer wavelengths should penetrate the cloud cover with very little attenuation. In an experiment from a spacecraft in the vicinity of Venus, one might also wish to choose a wavelength which is sensitive to a discontinuity in the space surrounding the planet; it may then be possible to measure the thickness of the cloud cover through observance of reflections at the boundary layer.

Ideally, one would like to obtain a high-resolution radar map of the planetary surface as the spacecraft moves in the vicinity of the planet. Data for constructing such a map may be derived either through use of brute-force conventional radar techniques or more sophisticated methods, such as radars using a synthetic-aperture antenna. At the time goals for this project were set, it appeared that the complexity of synthetic-antenna radars would prevent their use in an on-board experiment; hence, emphasis was placed on the development of a radar-type instrument of the simplest form. In view of this decision, it is recognized that the resolution capability of the instrumentation is degraded from that of a synthetic-antenna instrument, other factors being the same. Nevertheless, it was believed that some general statements about planetary-surface roughness can be made from measurements derived from a simple instrument and this has been borne out through aircraft flight tests of a rather simple instrument. Results of these tests are summarized in Section V.

The magnitude of microwave backscatter from objects depends in part on the roughness of the reflecting surface, its moisture content, and the angle of the impinging radiation. For normal incidence, smooth,

liquid surfaces return more energy per unit of impinging energy than does a rough, solid surface. Also, in the case of smooth, liquid reflectors, their reflective characteristics are much more sensitive to viewing angle than are solid surfaces. Furthermore, the backscatter properties of solid surfaces depend upon the nature of the surface and the degree of surface roughness. Thus one may expect substantial differences among backscatter measurements from smooth desert-like terrain, mountainous terrain, lakes, rivers, and so forth. These differences are accentuated when measurements are compared for a variety of different angles of arrival of the impinging electromagnetic illumination.

The problem of implementing an instrument that will make planetary backscatter measurements from a spacecraft under a variety of viewing angles is that of reconciling the many constraints imposed by spacecraft trajectory, expected miss distance, characteristics of the planetary surface, instrument sensitivity and measurement-accuracy requirements. For example, if the spacecraft is on a Venus fly-by trajectory, uncertainties in navigation and guidance could lead to uncertainties in miss distances of plus or minus several thousand kilometers. Since a radar instrument of the type being discussed has a sensitivity which involves the fourth power of distance between instrument and planet, a system that has a long-range capability and a wide dynamic range is required. On the other hand a different set of requirements may be imposed if the spacecraft is in a planetary orbit. At the time of initiation of this project, emphasis was on fly-by trajectories and this type of mission shaped the thinking of the group.

B. SPACECRAFT-RADAR MEASUREMENT SYSTEM

It is possible to employ a radar-type instrument to measure the scattering coefficient of a surface that reflects electromagnetic radiation. This coefficient is defined as the ratio of power backscattered by the target to that which would be backscattered by a perfectly reflecting, hemispherical isotropic scatterer. When all the radiated energy impinges on the reflecting surface, scattering coefficient may be expressed in the form

$$\Gamma(\theta) = \frac{2\pi R^2 W_r}{A_e W_t} \qquad (1)$$

$\Gamma(\theta)$ is the average scattering coefficient over the surface patch illuminated by the antenna beam.

θ is the angle between the horizontal plane tangent to the surface patch and the antenna bore sight axis ($\theta = 90^o$ represents normal incidence, see Fig. 1a).

R is the slant range between the radar and the surface.

W_t is the energy in the transmitted pulse.

W_r is the energy in the echo pulse.

A_e is the effective receiving area of the antenna.

The concept of a scattering coefficient as a measure of surface characteristics applies primarily to surfaces which act as diffuse scatterers over the antenna beamwidth. For nondiffuse scatterers, that is, specular surfaces or those with only a few isolated strong scatterers within the beam width, the scattering coefficient is also useful.

Measurements of $\Gamma(\theta)$ can be made for a range of incidence angles by illuminating the surface patch at a number of discrete viewing angles, as depicted in Fig. 1a.

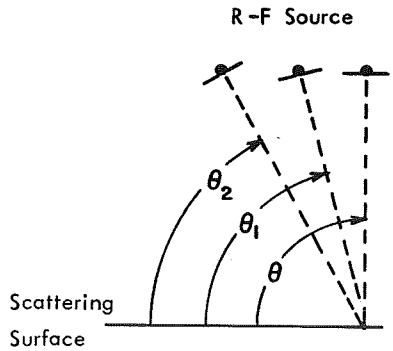

(a) Definition of Angle θ

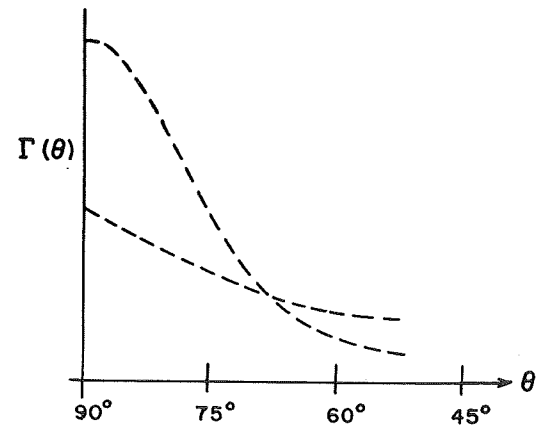

(b) Representation of the Scattering Coefficients of Two Hypothetical Surfaces

Fig. 1 Geometry Associated with Measurements of $\Gamma(\theta)$

In practice it is difficult to make measurements at various angles of incidence over exactly the same surface strip. Since most surfaces are reasonably homogeneous over some distance, however, it is possible to compare the results taken from separate measurements over the same general area. In addition, the effect of the finite antenna beamwidth is to smooth local variations.

A sketch which qualitatively represents the scattering coefficient of two hypothetical surfaces is shown in Fig. 1b. The shape of the curves in Fig. 1b depends on the characteristics of the surface and also on certain radar parameters. Since the objective is to ascertain surface characteristics from curves such as those shown in Fig. 1b, it is necessary to know the effect of the radar parameters such as the frequency, beamwidth, and so forth. A practical way of determining these effects is to measure the scattering coefficient of surfaces whose gross characteristics are known and to use these data as a calibration for measurement of unknown surfaces.

C. INSTRUMENT PARAMETERS

During the implementation of the overall research program, three types of experiments were considered:

1. A CV-990 aircraft experiment. This experiment was intended to permit evaluation of a specific radar as an instrument for measuring scattering coefficient, and to provide a basis for evaluating the usefulness of scattering coefficient measurements as means for describing surface roughness.

2. Earth-orbiting satellite experiment. The purpose of this experiment was to obtain calibration data for Venus experiments.

3. Venus experiment. This measuring system was designed for a Venus fly-by or orbiting spacecraft to explore the surface of Venus.

The configuration of the instrumentation for each experiment was the same; however, certain parameters had to be modified in order to accommodate various range conditions. Parameters that are special for each system are shown in Table 1. The r-f frequency in all cases approximates 10 GHz.

Table 1

Instrument Parameters for Three Types of Experiments

System Parameter	Experiment		
	Aircraft	Earth-Orbit	Venus Fly-by
R-f peak power	400 w	1000 w	7000 w
Maximum range	35,000 ft.	500 miles	3000 miles
Antenna beamwidth	8^{o}	8^{o}	0.7^{o}

At the completion of the program only the first type of experiment had been carried out.

The transmitter waveform that is appropriate for instrumentation of this kind is shown in Fig. 2. Time durations a, b and c should be

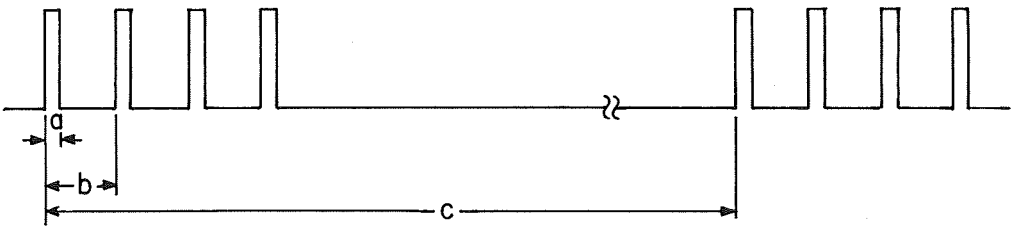

Fig. 2 Transmitter Waveform

given different values, depending upon the environment in which the experiments are conducted. Thus, for the instrument design being considered here, typical values are:

Experiment	Time Duration
Aircraft[1]	a = 40 microseconds b = 20 milliseconds c = 8 seconds
Earth Orbit[8]	a = 1 millisecond b = 15 milliseconds c = 17 seconds

Venus fly-by[6]	a = 200 microseconds b = 12 milliseconds c = 1.2 seconds

D. INSTRUMENT CONFIGURATION

Figure 3 is a simplified block diagram of the radar instrument for each class of experiments.

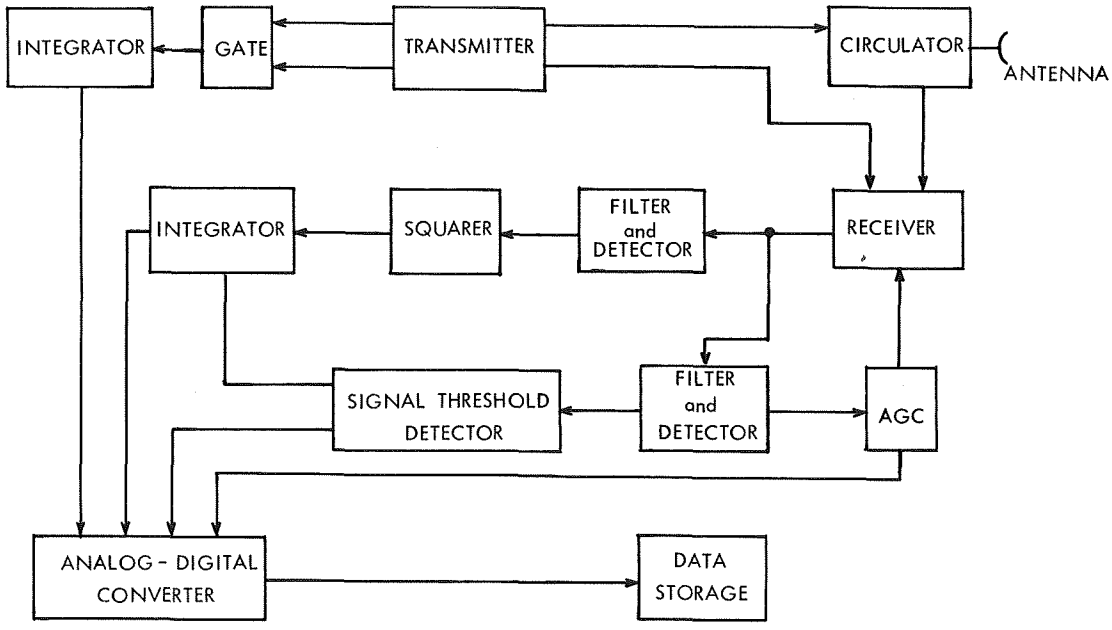

Fig. 3 Simplified Block Diagram of the Radar Instrument

Calculation of the scattering coefficient through use of Eq. 1 requires knowledge of the energy transmitted, energy received, range, and antenna aperture area. The energy transmitted, energy received, and range are measured for each pulse by the radar; the antenna aperture is a constant which may be calculated in two ways: from the measured gain of the antenna, and by integration of the area under E- and H-plane antenna-pattern measurements.

Range is proportional to the time between the leading edge of the transmitted pulse and the time when a detected echo pulse exceeds a threshold level. In the instrument this time is measured by counting the number of clock pulses in the time interval.

The energy transmitted is measured by detecting a sample of the transmitter-power output by means of a diode detector. This diode detector must be linear over a narrow range of power inputs so that its voltage output is proportional to power input. The detected voltage is integrated, converted to a binary number, and stored. The storage medium depends on the class of experiment being performed; for the aircraft experiment paper tape was employed.

The echo-signal-energy measurement is performed on an amplified replica of the energy received at the antenna terminals. The signal received at the antenna terminals is translated in frequency to 30 MHz and amplified in a linear i-f amplifier. The gain on the i-f amplifier is controlled by an AGC circuit which can be adjusted in 3-dB steps over a 42-dB range. The voltage output of the i-f amplifier is envelope-detected, squared, integrated, A-to-D converted and stored. The gain of the i-f amplifier is adjusted so that the voltage output of the squarer does not saturate, and the AGC setting required is recorded.

III. SUB-SYSTEM DEVELOPMENTS

The radar-instrument configuration used in the CV-990 aircraft experiment is shown in Fig. 4. The instrument may be divided into three basic units: transmitter, receiver, and data processor. The transmitter provides conditioned r-f power to illuminate the surface of interest so that the energy scattered backward from the target area can be measured. The receiver and data processor enable the measurement of the variables required to calculate the scattering coefficient. The data processor carries out an analog-to-digital conversion of the variables and calibration signals. In the design of instrument subsystems, primary importance was placed on reliability, light-weight, low-power consumption, and the use of available components where possible.

A. TRANSMITTER

The transmitter that was chosen consists of a light-weight klystron amplifier driven by a varactor chain. The transmitter unit as a whole includes, in addition to the klystron, filament circuitry for the klystron, a modulator to provide the klystron with the required pulse voltages, the necessary d-c to d-c converter-regulators to condition the prime power, and the r-f transmission line with the required switching components.

1. Klystron

The tube specification shown in Table 2 and Fig. 5 were submitted to several suppliers. Varian Associates were chosen as the supplier.

The first tube constructed by Varian Associates was designated VA-909; it utilized a Philips dispenser-type cathode. Initially, the tube showed evidence of being gassy and it consumed more than the 8 watts specified value of filament power. During run-in there was no undue sparking, gas cleared up and the heater power gradually came down.

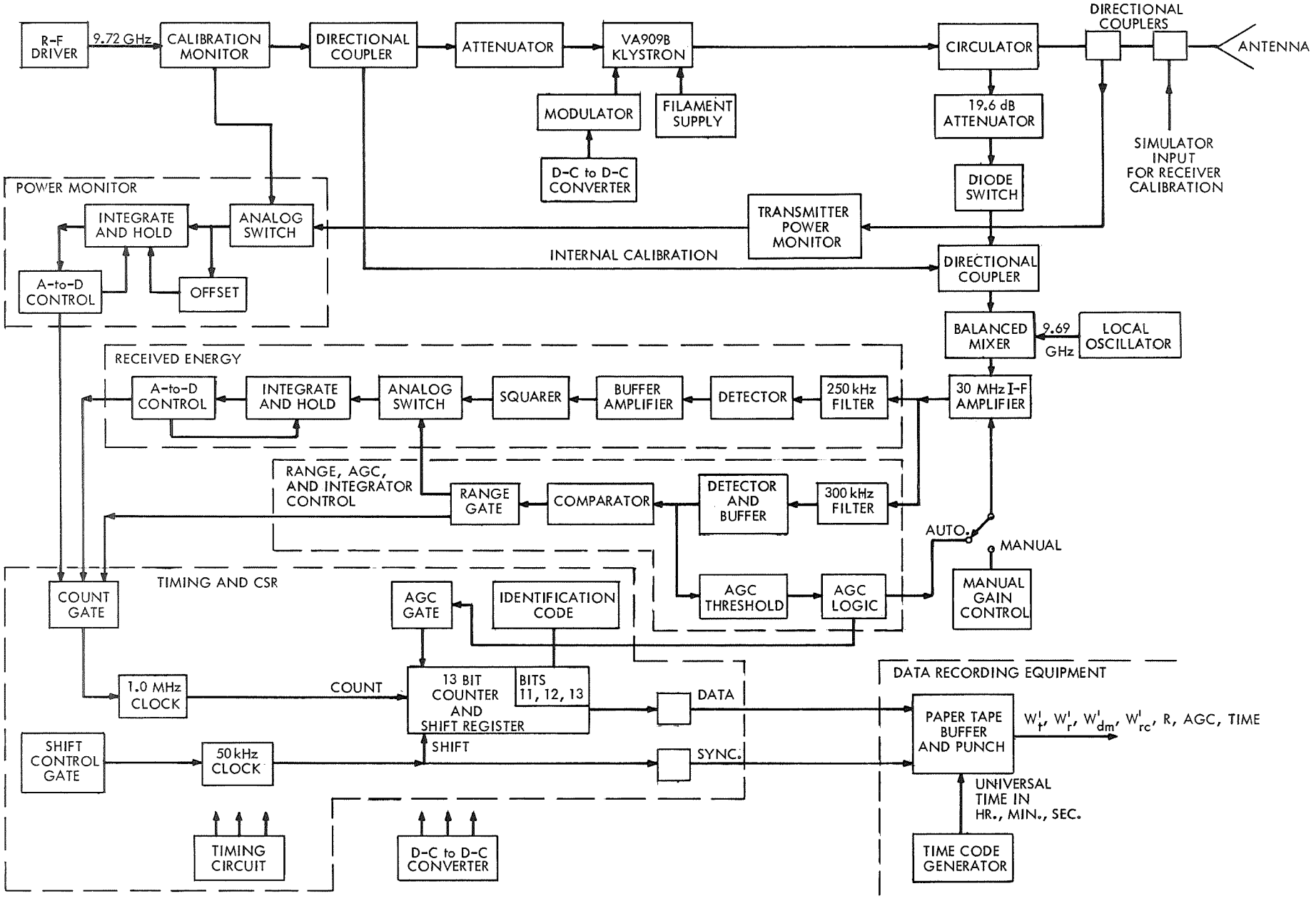

Fig. 4 Detailed Block Diagram of Radar Instrument Used in the CV-990 Experiment

At the completion of the test period, power required by the heater to obtain full r-f power output was nine watts. Otherwise, the tube operated satisfactorily and met other specifications.

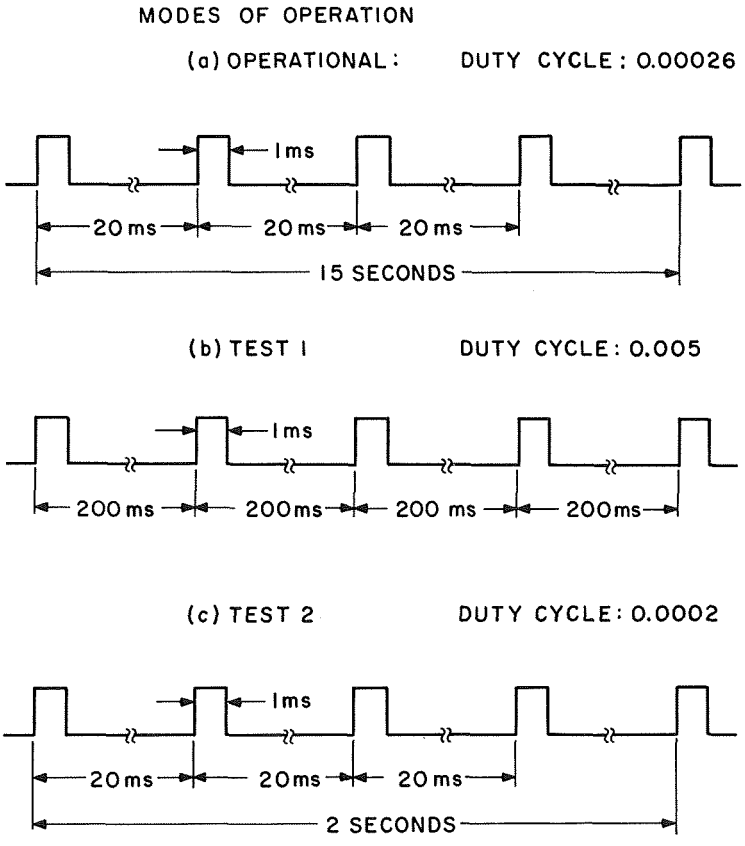

Fig. 5 Waveform Specification

In this initial attempt to meet the eight-watt filament requirements the cathode support cylinder was constructed to reduce conduction heat loss and a shield was used to reduce ratiation heat loss. Implementation of these designs resulted in the power requirement of nine watts.

Table 2

Electrical and Physical Specifications of Klystron Transmitter

	Typical	Minimum	Maximum
Center frequency	9.72 GHz		
Tuning	9.72 GHz	9.695 GHz	9.745 GHz
Heater voltage	5.75 V(rms)		6.0 V(rms)
Heater power			8.0 W
Heater surge current			3 A for 30 sec.
Heater warm-up time		120 sec.	
D-C beam voltage	7.5 kV		8.0 kV
Peak beam current	0.60 a		0.65 a
Driver power	20 mW		30 mW
Gain			
Synchronously tuned	50 dB	48 dB	
Efficiency-tuned	43 dB	40 dB	
Efficiency			
Synchronously tuned	25%	24%	
Efficiency-tuned	30%	27%	
Bandwidth (3-dB points)	10 MHz	8 MHz	
Load VSWR	1.25:1		1.25:1
Mounting position	any		
Vibration (nonoperating)	20 g at 20 to 1KHz all planes		
Objective	20 g at 20 to 2KHz all planes		
Shock and acceleration	Duration, 10 millisec		
	10 g linear, all planes		
Temperature cycling (nonoperating)	-20°C to +80°C		
Ambient temperature (operating)	+15°C to +30°C		
Weight:			
Objective	Less than 5 pounds		
Maximum	5-1/2 pounds		
Input-Output	Waveguide, Flanges mate with UG-39/U		
Cooling	Conduction through mounting to housing		
Life			
Expectancy	5000 hours		
Warranty	500 hours		

It became evident during the program that an attempt should be made to improve the klystron cathode. Varian was requested to continue their cathode investigations and to make another attempt to meet the filament power specification of eight watts. As a result, a new approach was tried which held promise of reducing filament power below the eight watts specified. The main feature of this new approach was an oxide type of cathode. This cathode type is normally used in tubes that operate at short pulse lengths, typically less than 10 μsec. Oxide cathodes are susceptible to effects of ion bombardment and for this reason are not used when ion bombardment may occur. When the pulse duration is shorter than the time required for ion-current formation, no ion bombardment occurs. Since on this application the VA909 must operate at a maximum pulse width of one millisecond, an oxide cathode would generally not be considered. However, a new technique to reduce the effect of ion bombardment was incorporated into the tube in the belief that it would work well.

This second tube was tested extensively. Proper beam current performance was obtained with only six watts of heater power. No changes were apparent in the beam current or heater characteristics. The tube is designated the VA-909B and is illustrated in Fig. 6.

The VA-909B was delivered during June, 1967, and a series of tests were conducted on it. The results are shown in Fig. 7. In summary, the tube operated satisfactorily. At the conclusion of the tests the tube was installed in the aircraft flight-test instrument for system evaluation test and calibration measurements. During this period the tube was operated at a 40-microsecond pulse width. This pulse width was necessary because the maximum altitude at which the aircraft instrument could be flown was to be approximately 40,000 feet.

In September 1967, after approximately 100 hours of operation, the klystron power output gradually decreased and leveled off at about 500 watts peak power. No attempt was made to modify filament voltage or other parameters during this period to increase the power.

Following operation in the laboratory, the entire instrument was brought to NASA Ames Research Center, Moffet Field, California, and

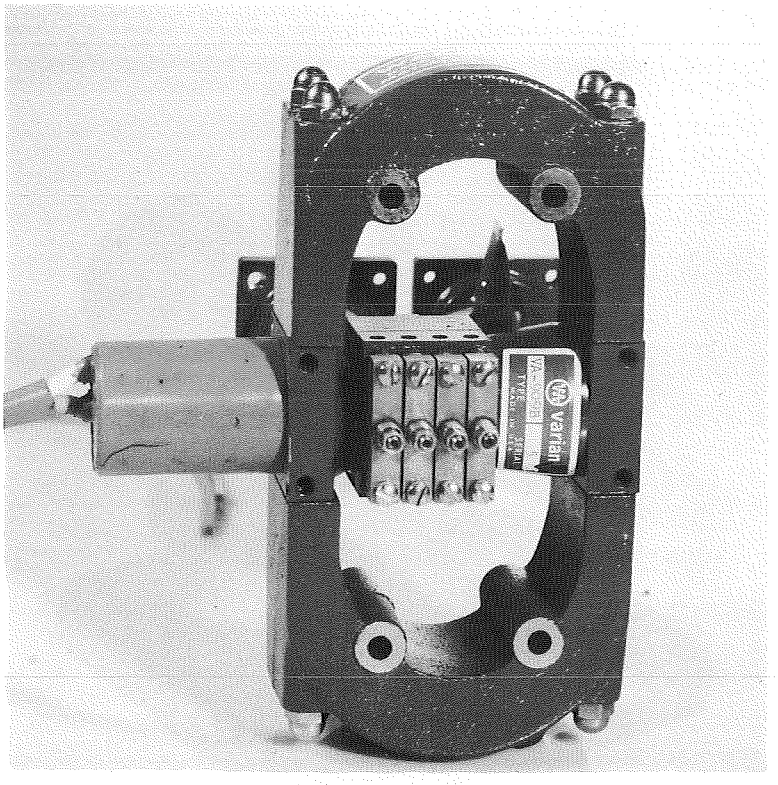

Fig. 6 VA-909B Klystron

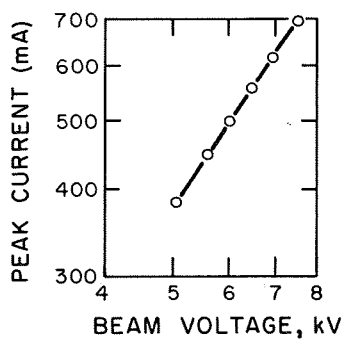

(a) Peak Current vs Beam Voltage

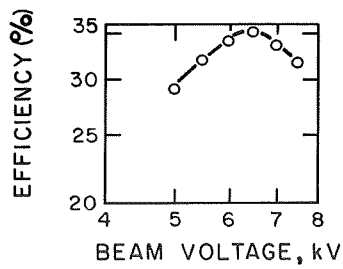

(c) Efficiency vs Beam Voltage

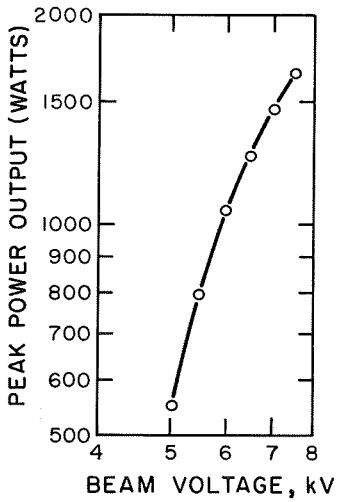

(b) Power Output vs Beam Voltage

Note:
HEATER = 3.8 V @ 1.80 amps.
F_o = 9.720 GHz

Fig. 7 Characteristic Curves of the VA-909B Klystron

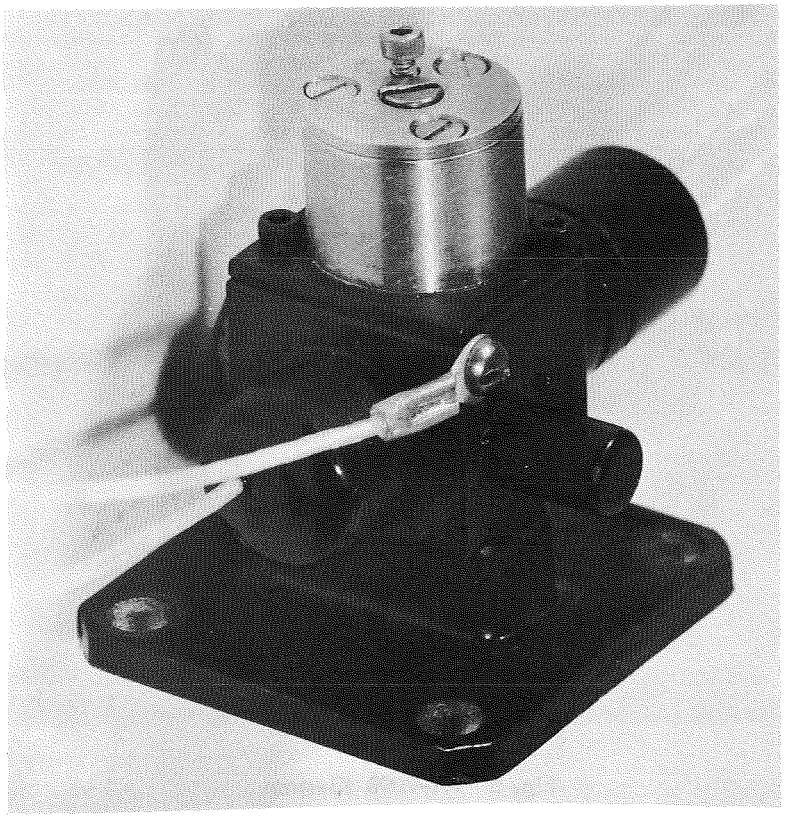

Fig. 8 Type MXK-73 Klystron Oscillator. Weight 5-1/2 oz; R-F Output Power, 85 Milliwatts; Heater Power, 8 Watts.

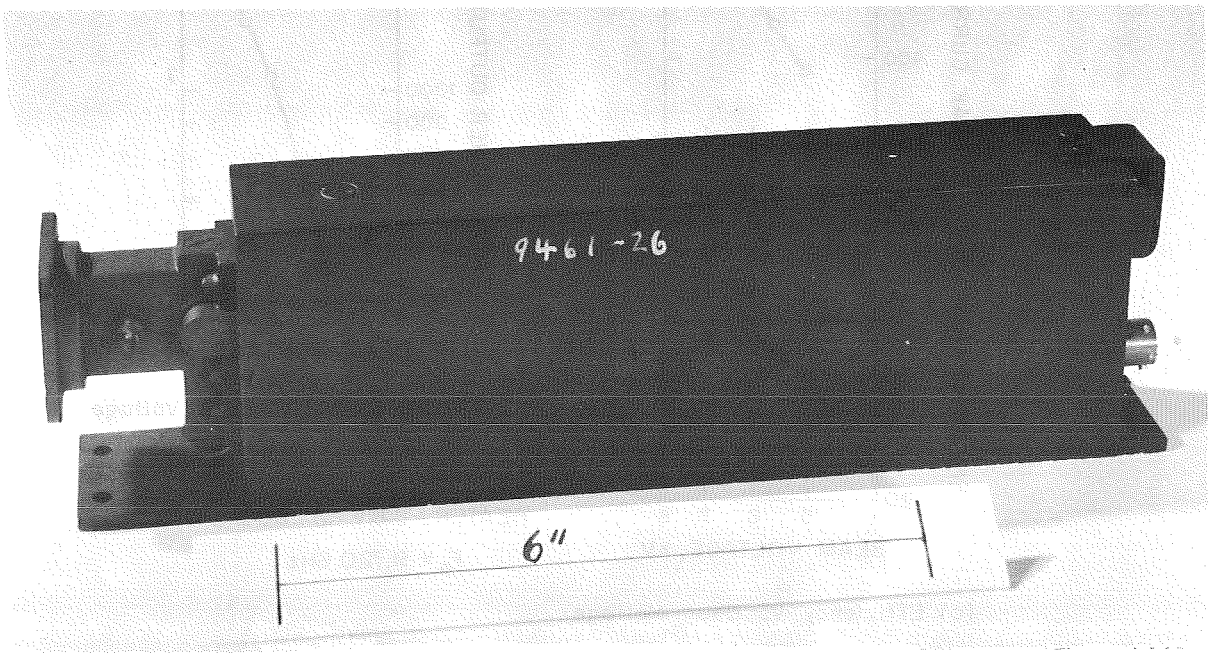

Fig. 9 Varactor Harmonic Generator

installed in the NASA Convair 990 aircraft. Flight tests were conducted on October 10, 11, 12, 1967. The klystron r-f output was constant at 500 watts, peak, during the tests.

At the conclusion of the flight-test program, the tube was delivered to Varian for further testing. They determined that cathode emission was, indeed, low and a replacement cathode was installed in the tube.

2. Varactor-Multiplier Chain

Two possibilities were investigated as sources of r-f driving power for the VA-909B. One approach makes use of an X-band klystron oscillator of the type illustrated in Fig. 8. Another approach uses a 101 MHz crystal-controlled transistor oscillator followed by a solid-state varactor-multiplier chain. Power consumption is an important consideration in each case. The varactor chain required 24 watts of input power to obtain 80 milliwatts of X-band r-f output power under c-w conditions. On the other hand, anode power consumption by the klystron driver is low, but heater power is appreciable, and the ability to cycle the heater supply between full value and 25 to 50 percent rated value was uncertain. Since the main power supply of the harmonic chain can be cycled between full-on and full-off without impairment of performance (see below), and since the chain has high-frequency stability, this approach was selected for the radar instrument.

To avoid possible difficulties from spurious oscillations that might occur if local-oscillator power is derived from the transmitter harmonic chain, two separate sources of r-f power were used - one to drive the power klystron and the other to supply local-oscillator power to the receiver.

The varactor harmonic generator is illustrated in Fig. 9. Characteristics of the transmitter and local-oscillator units are as follows:

Transmitter Unit

Output Frequency	9.720 GHz
R-f Output Power Variation	80 milliwatts
D-c Input Power (not pulsed)	24 watts
Output-Power Stability	$< \pm$ 1 dB between -10°C and +5°C
Spectral Purity	
Amplitude of signals at harmonics of operating frequency	at least 50 dB below operating frequency
Amplitude of signals at spurious frequencies	at least 50 dB below operating frequency
Weight	2-1/4 lbs.

The local-oscillator chain has similar characteristics except that it operates at 9.69 GHz and has an output power of 12 mW. It should be noted that the varactor harmonic generators used in the instrument and described above are 1966 vintage. Advancements in the technology since then should yield a smaller, lighter weight package.

Operation of the harmonic chain on an intermittent-duty basis is of prime importance in order to reduce power consumption. Since no data were available concerning behavior of the device under this type of operation, extensive tests were conducted. In the tests, the 101-MHz crystal oscillator was allowed to operate c-w, and the succeeding amplifiers were pulsed. Pulsing was accomplished by turning the power-supply voltage on and off. The waveforms of Fig. 10 show the nature of the buildup of the envelope of the r-f output signal when a 28-volt pulse is applied to the d-c power supply terminal for the amplifiers. The bottom waveform is the 28-volt power-supply pulse and upper-two waveforms are envelopes of the r-f output pulse. It can be observed that a delay of approximately 1.25 microseconds occurs before oscillations commence buildup and that the time constant of buildup is of the order of 5 microseconds. Fortunately, the buildup time is unimportant in this application because of the long-duration pulses being employed, and the delay in start of oscillations can be circumvented by initiating the d-c supply pulse for the varactor chain a few microseconds before power is applied to the transmitter tube.

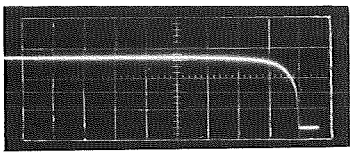

← Time

Envelope of R-F Pulse
Showing Rise Time.

Scale: 5.0 μsec/div

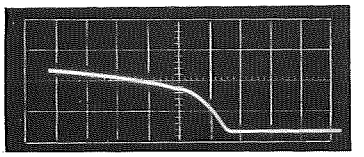

← Time

Envelope of R-F Pulse
Showing Rise Time and
Delay from Voltage Pulse.

Scale: 0.5 μsec/div

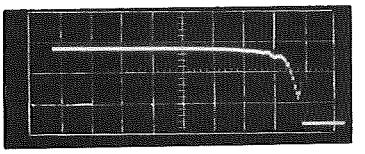

← Time

The 28-volt Power-Supply
Pulse.

Scale: 0.5 μsec/div

Fig. 10 Waveforms Showing the Buildup Time of R-f Output Signal from Varactor Harmonic Generator under Pulsed Power-Supply Conditions

As a result of being able to pulse the power supply to the varactor generator, the power requirement for the chain can be reduced to approximately 4 percent of its c-w value, that is, from 24 watts to 1.0 watt.

3. Modulator

The purpose of the modulator is to convert a low voltage (400 volts, d-c)to a high voltage pulse (8 kV) suitable for switching the beam current of the klystron. The design is somewhat complicated by the requirement for a burst of pulses which in turn demands high peak power. In addition, the normal pulse width of one millisecond tends to increase the weight of any magnetic components that may be employed.

Several alternative configurations were initially considered of which two were chosen for construction and evaluation. The two methods are:

> Discharge of a pulse-forming network utilizing linear ferrite core inductors through a silicon-controlled rectifier.[25,29]
>
> Switching the primary of a step-up transformer by means of high-voltage transistors.

The first method yielded a modulator whose weight, including the pulse-forming network, charging inductor, pulse transformer, and silicon-controlled-rectifier switching circuit was approximately 10 pounds; it operated at an efficiency of about 75 percent.

When high-voltage switching transistors became available, the second configuration was designed, constructed, and incorporated into the final system design. A simplified schematic is shown in Fig. 11. This design derives the high-voltage pulse for the klystron from the secondary of a step-up transformer whose primary is switched by three high-voltage transistors in parallel. The resistors R_e in the emitters of the high-voltage transistors Q_1, Q_2 and Q_3 ensure that the current in the transistors are equal. The high-voltage transformer is reset through a third-winding by means of transistor Q_4 in order to achieve a lower weight and size for the transformer. There is also protective circuitry, not shown in the modulator diagram, which protects the high-voltage transistors in the event of arc-over in the klystron. The modulator operated satisfactorily during all laboratory and flight testing.

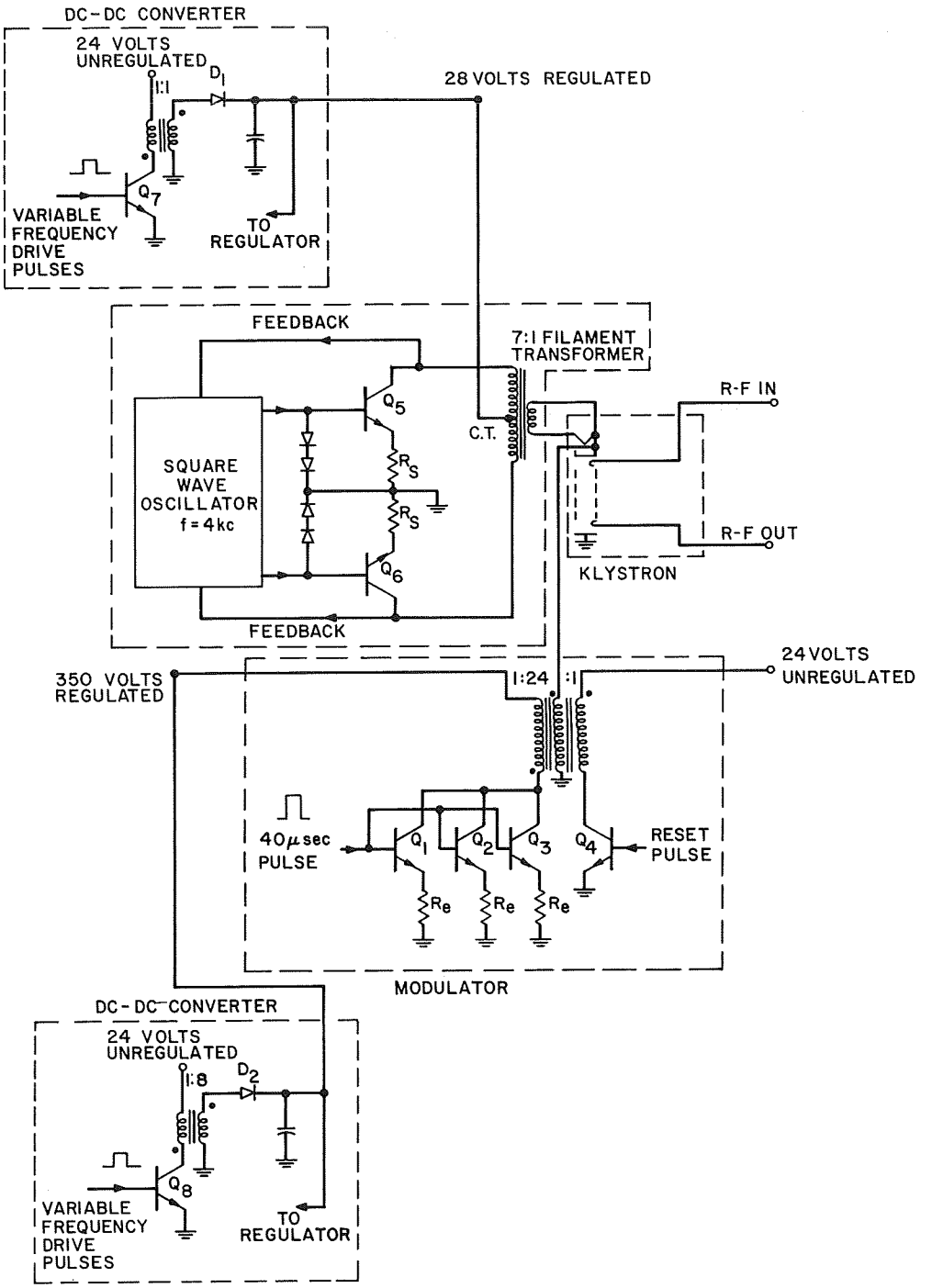

Fig. 11 Simplified Schematic Diagram of Modulator

Transformer weight was 16 ounces and was contained in a 2.5 in. x 2.5 in. x 3 in. package.

4. High-Power, High-Voltage Converter[3]

A simplified schematic diagram of the 24-v to 400-v converter which supplied the radar modulator is shown at the lower left on Fig. 11, and the complete schematic diagram is drawn in Fig. 12. The transmitter pulse profile is such that approximately 300 watts are required for a 100-millisecond interval, followed by a period lasting from one to ten seconds during which no power is required.

The converter operates from an input voltage between 23 and 33 volts. The stand-by power required is 15 mw, and an incremental efficiency of 80 percent is obtained. Regulation for this converter is within $\pm$ 2 volts (including ripple) for temperature changes from 0° C to $\pm$ 50° C. The weight of the equipment, which can operate continuously at the 300 watt level if necessary, is less than five pounds.

5. Power-Monitor Channels

The transmitter-energy monitoring channel consists of a calibrated directional coupler located in the r-f line preceding the antenna. The coupler furnishes a sample of transmitted power to a calibrated diode detector, (Refer to Fig. 4.) The r-f power used to monitor the gain stability of the receiving channel is obtained by extracting a portion of the r-f driver output through calibrated directional couplers and inserting the power in the mixer at the conclusion of echo-pulse reception. The r-f driver output is also monitored by means of a calibrated detector.

Each power-monitor diode provides an output voltage that is related to the r-f power incident on the monitor diode. A dual-input analog switch is controlled by the timing circuits to connect the proper power-monitor input to the integrator during the calibration times. The output of the gated integrator is designed to be proportional to the calibration-signal energy. At the end of the transmitter calibration pulse, the gated integrator switches to a HOLD mode, and the voltage is A-to-D converted.

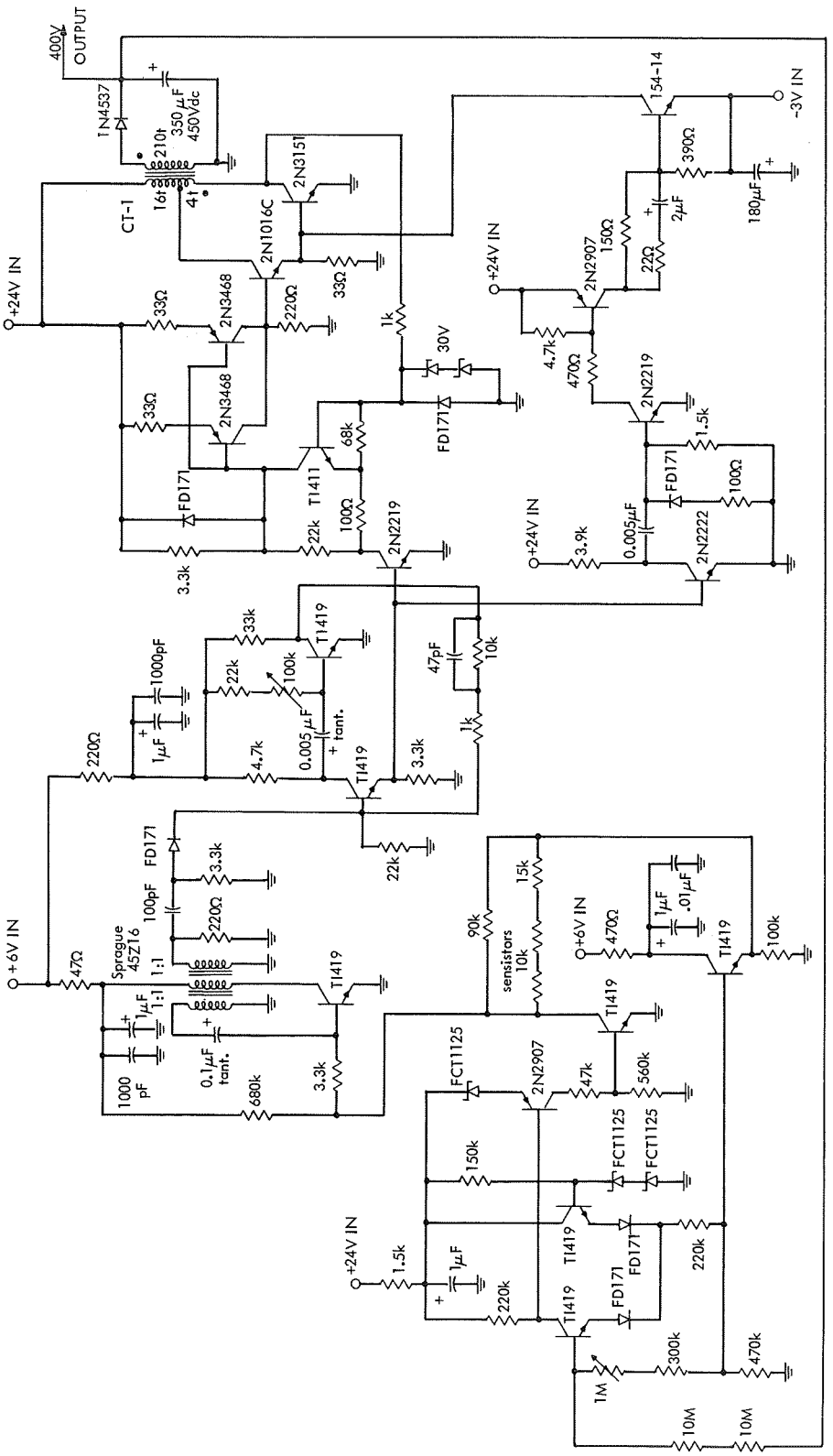

Fig. 12 High Power DC - DC Converter

B. RECEIVER

The solid-state receiver module originally selected for use in the radar-instrument system was a purchased item, one of the first to become available on the commercial market. The module consisted of a tunnel-diode r-f amplifier, a notch filter, a balanced crystal mixer, and a 30-MHz transistor i-f amplifier. The use of a tunnel-diode r-f amplifier is desirable in the configuration of the system that is intended to observe Venus since a 6-dB improvement in signal-to-noise ratio can be realized over that of a conventional system employing a mixer input circuit.

1. Tunnel-Diode R-f Amplifier

When it was determined that the flight-test program using the NASA CV-990 aircraft was to be undertaken, a comprehensive calibration and evaluation program was initiated. This phase of the program disclosed several system deficiences, and several subsystem and calibration equipment modifications were required.

The tunnel-diode r-f amplifier was found to generate noise over a wide band of frequencies that included the desired signal passband and the image-frequency passband. Noise at the image frequency is not acceptable since it converts to the intermediate frequency and a 3-dB degradation in noise figure is obtained. A narrow-band image-rejection filter having a loss of about 15 dB at the image frequency was placed after the tunnel-diode amplifier to remove this noise. Changes in ambient temperature of the order of 20° to 35° C affected the extremely frequency-sensitive circuits and reliable calibration data were impossible to obtain. In addition, the r-f amplifier was poorly shielded and thus the unit was susceptible to radio-frequency interference. Because of these problems, the urgency to complete the most comprehensive calibration program possible and because the improved noise figure obtained by use of the tunnel-diode amplifier was not necessary for an aircraft experiment, the entire tunnel-diode-amplifier assembly was removed from the system.

2. Intermediate-Frequency Amplifier

During system-calibration tests it became apparent that the X-band receiver lacked adequate gain stability and repeatability of gain versus AGC voltage. One source of these deficiencies was the receiver i-f amplifier which not only lacked a stable gain control, but also saturated at a power output 6 dB below the required maximum.

In order to overcome these problems, a new amplifier was designed and constructed in the Laboratory. The primary objectives of the new amplifier design were excellent gain stability and precise gain control. The new design featured a unique digital gain control formed by six electronically switched resistive attenuators.

A summary of the specifications of the i-f amplifier is given below and a block diagram of the amplifier is shown in Fig. 13.

Center Frequency	30 MHz
3-dB bandwidth	3 MHz
Power gain	110 dB
Noise figure	3 dB
Gain control	Digital: -42 dB in 14 steps, -3 dB each
Gain stability at 110 gain	$\pm$ 1/2 dB, 10°C to 40° C
Gain resetability	Limited only by overall gain stability

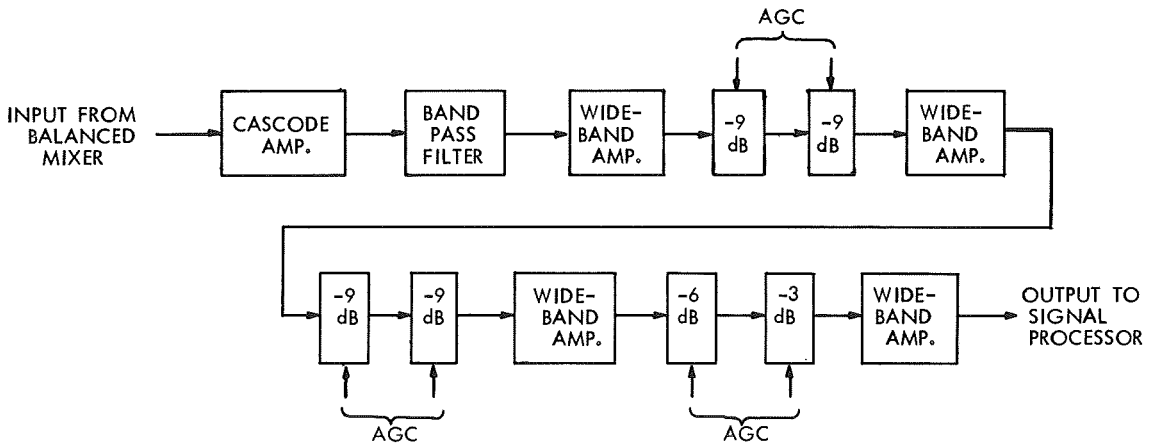

Fig. 13 Block Diagram of I-f Amplifier

Each stage of the i-f amplifier was designed to have a high degree of gain stability. The wide-band amplifiers are coupled through electronically switched resistive attenuators that are used to control the overall gain of the i-f amplifier. This system of digital AGC has several advantages over commonly used analog AGC circuits, particularly in the areas of calibration and resetability of gain. Because the gain is adjustable in a fixed number of discrete steps, it is practical to calibrate the receiver for all possible gain settings. In contrast, an analog AGC circuit produces theroretically an infinite number of gains, making it impractical to calibrate all gain settings. Further, the actual gain setting of the digital AGC is easily determined by noting the state of the switches that drive the attenuators.

Operation of the wide-band amplifiers and the attenuators are discussed in Reference 1.

3. Local Oscillator

The local oscillator is a varactor harmonic generator with the same characteristics as the r-f driver unit discussed in the transmitter section with the exception that the power output is 12 mw and the operating frequency is 9.69 GHz.

C. DATA PROCESSOR

The configuration of the data processor can be seen in the detailed block diagram shown in Fig. 4. Several functions are performed by the data processor. It permits calculation of the scattering coefficient by conditioning the receiver i-f amplifier output signal and a sample of the transmitter pulse energy; it provides for measurement of slant range from radar instrument to the scattering surface; and it performs an analog-to-digital conversion of these three quantities so that they may be stored in digital form at the instrument location. Data-processor average-power consumption is 200 mw for its 450 silicon transistors.

1. Receiver-Signal Channel

The i-f amplifier output is fed through the band-pass filters and envelope detector bank, as shown in Fig. 4. One filter and detector drives the received-energy channel and the other drives the signal

comparator and AGC threshold detector. The detectors are linear over a range of 30 mV to 2 volts, peak-to-peak and approximate the characteristic of an ideal linear detector. The received-energy channel next connects the detector output to a squarer circuit whose output voltage is proportional to the power in the backscattered signal. The output of the squarer in turn is connected to a gated integrator where the voltage held by the integrator is linearly proportional to the energy in the backscattered signal. When the echo signal ends, the magnitude of the voltage held by the integrator is converted to a 10-bit binary number representing the magnitude.

The comparator is fed from the detected output of the 300-kHz filter. It operates in conjunction with the range gate to control the gated integrator in the signal-energy channel just discussed.

The range clock is initiated at the beginning of a transmitter pulse. When an echo is detected, the range gate stops the clock whose pulses are counted by the counter shift register. The counter thus contains a binary number that is linearly proportional to range time or distance when the clock is stopped. The number can next be shifted out for recording.

2. Counter and Shift Register

The key element in the digital portion of the data processor is a 13-bit counter and shift register, (CSR). The CSR is time-shared by all 13 analog-to-digital conversions that are carried out during each burst of four pulses. The time-sharing is accomplished by sequencing the A-to-D conversions that involve the variables W_t', W_r', and W_{rc}' that are stored in the gated integrators. The range time is obtained directly in digital form as discussed previously, and is therefore the first quantity shifted from the CSR after the last three transmitted pulses in a burst. The AGC setting (that is, the state of the six AGC switches) is stored in digital form in the AGC logic circuits and is transferred on command to the CSR.

At the end of each A-to-D period, the CSR contains a binary number with a maximum of 10 bits (1023 decimal magnitude) that is proportional to the variable being measured. After every A-to-D period, the last three bits of the CSR are set according to the command of the identifying

code matrix, and all 13 bits are shifted serially out of the CSR at a 50-kHz rate. The 13-bit word is stored in a paper-tape punch buffer, and then punched onto paper tape. A diagram of the data-output sequence is shown in Fig. 14.

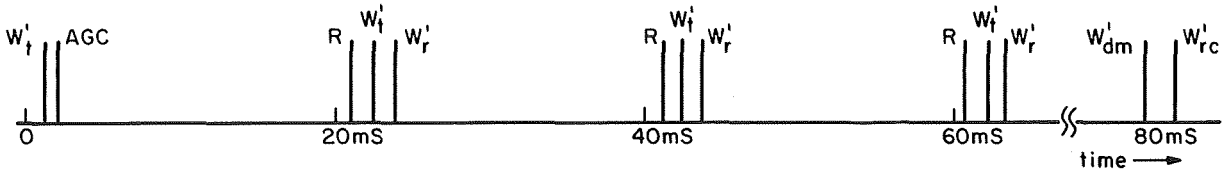

AGC = Automatic Gain Control
R = Range
W'_t = Energy Transmitter
W'_r = Energy Received
W'_{rc} = Receiver Calibration Energy
W'_{dm} = Driver Monitor

Fig. 14 Data-Output Sequence

IV. CALIBRATION PROCEDURES

A. R-F SIMULATOR

The necessity to test, evaluate, and calibrate the radar measuring instrument in the Laboratory led to the design and construction of an X-band simulator.[4,21] A block diagram of the simulator is shown in Fig. 15.

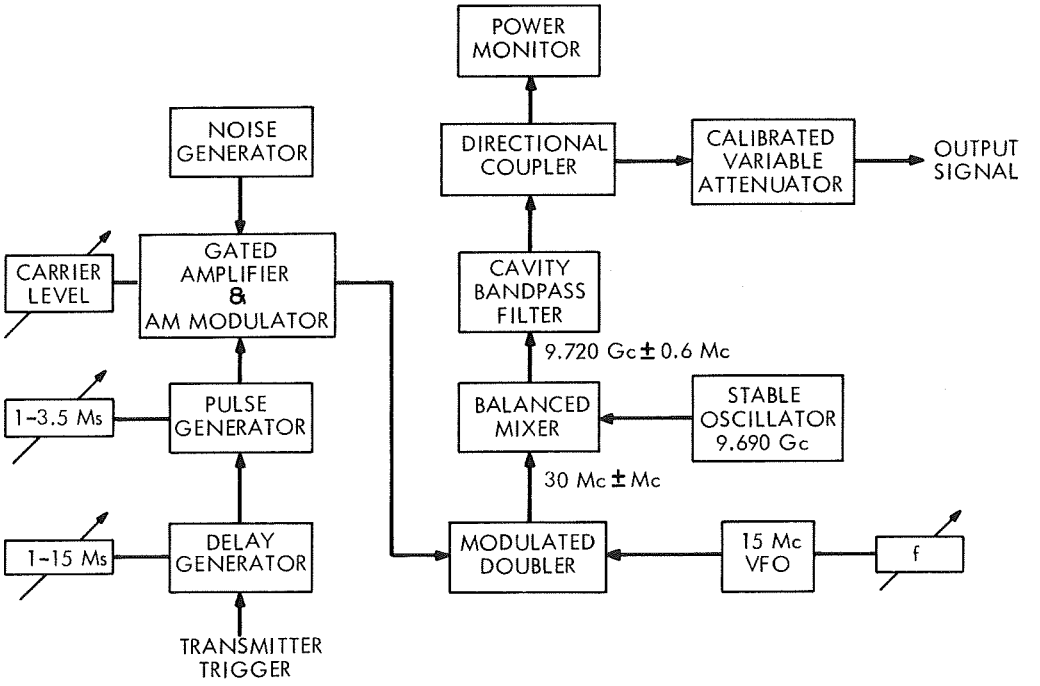

Fig. 15 Doppler Simulator Block Diagram

In order to attain the required r-f stability while retaining the feature of continuous tuning over a 1.2-MHz band, a method of up-conversion using a stable 9.690-GHz source and a variable 30-MHz source was adopted. The frequency stability of the simulator is thus determined by the stability of the fixed-frequency microwave source. The 30-MHz source need not have stability much better than 1 part in 10^3 to contribute negligible error. Also, it can be varied in frequency and either amplitude or frequency-modulated.

The 30-MHz signal is up-converted to 9.720-GHz through use of a balanced modulator which suppresses the carrier by more than 20 dB. The modulator output is passed through a single-cavity bandpass filter which further rejects the carrier by 22 dB and rejects the unwanted sideband at 9.660-GHz by 29 dB. These unwanted frequencies could lead to error in the simulator output power calibration using a broadband power monitor. The 9.72-GHz signal is measured with a calibrated diode detector.

After passing through a directional coupler and a precision variable attenuator the signal is variable over a range from the minimum discernible signal to saturation of the receiving channel.

B. RADAR-INSTRUMENT CALIBRATION

Laboratory tests were undertaken to determine the accuracy and repeatability of the radar-measuring instrument in measuring the required quantities. These quantities are:

$$W_r = k_r W_r' \tag{2}$$

where

W_r is the received energy at the antenna terminals

k_r is the receiver-channel calibration factor

W_r' is the received energy measured at the data processor output

and

$$W_t = k_t W_t' \tag{3}$$

where

W_t is the transmitted energy

k_t is the transmitter-channel calibration factor

W_t' is the transmitted energy measured at the data processor output

The purpose of the laboratory calibration is to determine the conversion factors k_r and k_t. The measurement accuracy and degree of measurement repeatability can be determined during the calibration procedure.

1. Transmitted Energy W_t

The energy transmitted is measured by detecting a sample of the transmitted power with a point-contact diode detector and integrating the detected voltage, as previously discussed.

2. Calibration of Receiving Channel

The calibration procedure for the receiving channel involves the use of the simulator, also previously described. The receiving-channel gain is measured by injecting an unmodulated pulse of known power level and duration at the input terminals of the instrument and recording the binary output representing the energy. This procedure is followed over the AGC range of the receiver and the recorded data are used to construct calibration curves shown in Fig. 16. The AGC

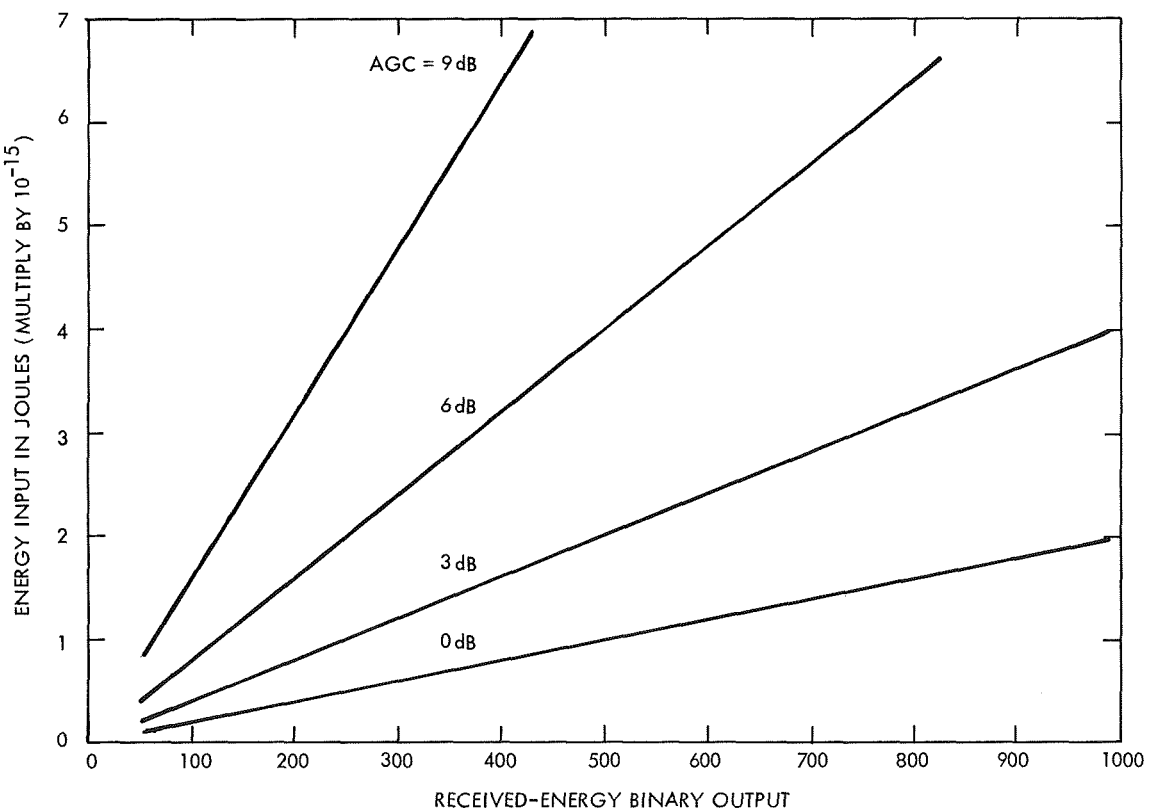

Fig. 16 Received Energy Calibration Curves

values indicate the amount by which the i-f amplifier gain is decreased; 0 dB means the i-f amplifier is at maximum gain. From knowledge of the AGC setting and measurements of the receiving binary output, the energy present at the antenna terminals is determined.

3. Gain Stability

An internal calibration signal of known energy is provided to check the gain stability of the receiving channel during operation of the radar measuring instrument. A small portion of the r-f driver output at 9.72 GHz is directed to the mixer input, as shown in Fig. 4, after all echo pulses have been received. AGC automatically sets to a known value and the receiving-channel gain is checked at one point. If the gain is constant, the binary output that defines the internal calibration energy remains constant. The output of the r-f driver is also monitored by means of a calibrated diode detector, integrated, A-to-D converted, and read in binary form.

4. Range Calibration

The accuracy of the range measurement is checked by observing the time interval between the leading edge of the transmitted and simulated echo pulses on a calibrated oscilloscope.

5. Measurement Accuracy

The radar instrument was checked periodically to insure that the calibration factors were constant. For signal-to-noise ratios greater than 6 dB and constant temperatures the measurements are repeatable to within ± 1 microsecond for range, ±1/2 dB transmitted energy, and ±1 dB for received energy. This results in scattering coefficient measurements being repeatable within ±1-1/2 dB.

V. FLIGHT TESTS

Flight tests on the radar instrument were conducted with the cooperation of NASA Ames Research Center, Moffett Field, California. Measurements were taken over selected target areas in the Western United States with the instrument installed in a NASA CV-990 airplane. The flight paths from which data were taken are shown in Figs. 17 and 18.

The purposes of flight testing, which was conducted Oct. 10-12, 1967, were twofold:

1. To evaluate the performance of the radar as an instrument for measuring scattering coefficients.

2. To observe the relationships between types of terrain and the scattering coefficients which are associated with the terrain.

Two reports on the results of the tests have been prepared. Reference 2 is a summary report and Reference 1 is a detailed report including a more exhaustive analysis of the data. The purpose of the experiment was accomplished and a productive amount of data on X-band backscattering properties from a variety of surfaces were recorded. Analysis of the data leads to the conclusion that gross surface features can be deduced by measurements of this kind. The rest of this chapter is devoted to a discussion of flight-test results as reported in References 1 and 2.

The flight configuration which was necessary to make the required microwave measurements was determined by several factors. The basic requirement was that the aircraft fly over the same target area several times; first, on a straight level course; second, at a bank angle of 15 degrees; and third, at a bank angle of 30 degrees. The reason for this flight configuration was to obtain information on the same general area at oblique as well as normal incidence.

Another requirement was that the weather be clear during the measurement periods to allow the camera, located near the radar antenna, to photographically record the area being measured by the

radar. Also, the type of target had to be easily distinguishable from an altitude of 35,000 feet. The antenna viewing area with the aircraft operating at this altitude was about one mile in diameter.

The areas of interest included smooth water, rougher water, both flat and rolling farmland, mountains and smooth terrain of the type found in certain desert areas.

After the completion of the flight tests the digitally encoded data stored on paper tape along with appropriate calibration factors were fed into a digital computer. The computer furnished a numerical printout of the quantities measured and from these quantities calculated the scattering coefficient which was recorded on both cards and magnetic tape. The computer printout was carefully examined and it was determined that approximately 40 percent of the data recorded was reliable and usable. The remaining data were unsable either because they fell outside the dynamic range of the receiving system or because of malfunctions in the data-recording system. In addition, the usable data were compared with the film record to insure that the flight path over a target area did not include terrain which was not representative of the target area. For example, if a small body of water appeared in the flight path over a target area which was predominantly farmland, the data from the water were not used.

The data remaining after these editing procedures are presented in graphical form in the set of figures that appear at the end of this chapter. Figure 19 shows the mean value of the scattering coefficient at the three angles at incidence of 90°, 75°, and 60° for each of the seven target areas. The data used to compute the mean values of scattering coefficient are plotted in chronological form in Figs. 20a through 27a and in the form of histograms in Figs. 20b through 27b. Data were taken at only 90° incidence from lava beds in Idaho and only single plots have been included for this area. Also, insufficient data were collected over Salt Lake to furnish a meaningful plot at 60°.

The figures portraying the values of Γ in Figs. 20a through 27a require explanation. The burst numbers shown on the horizontal scale refer to the data recorded during a specific four-pulse burst. A unit change in burst number (e.g., 796 to 797) represents a change

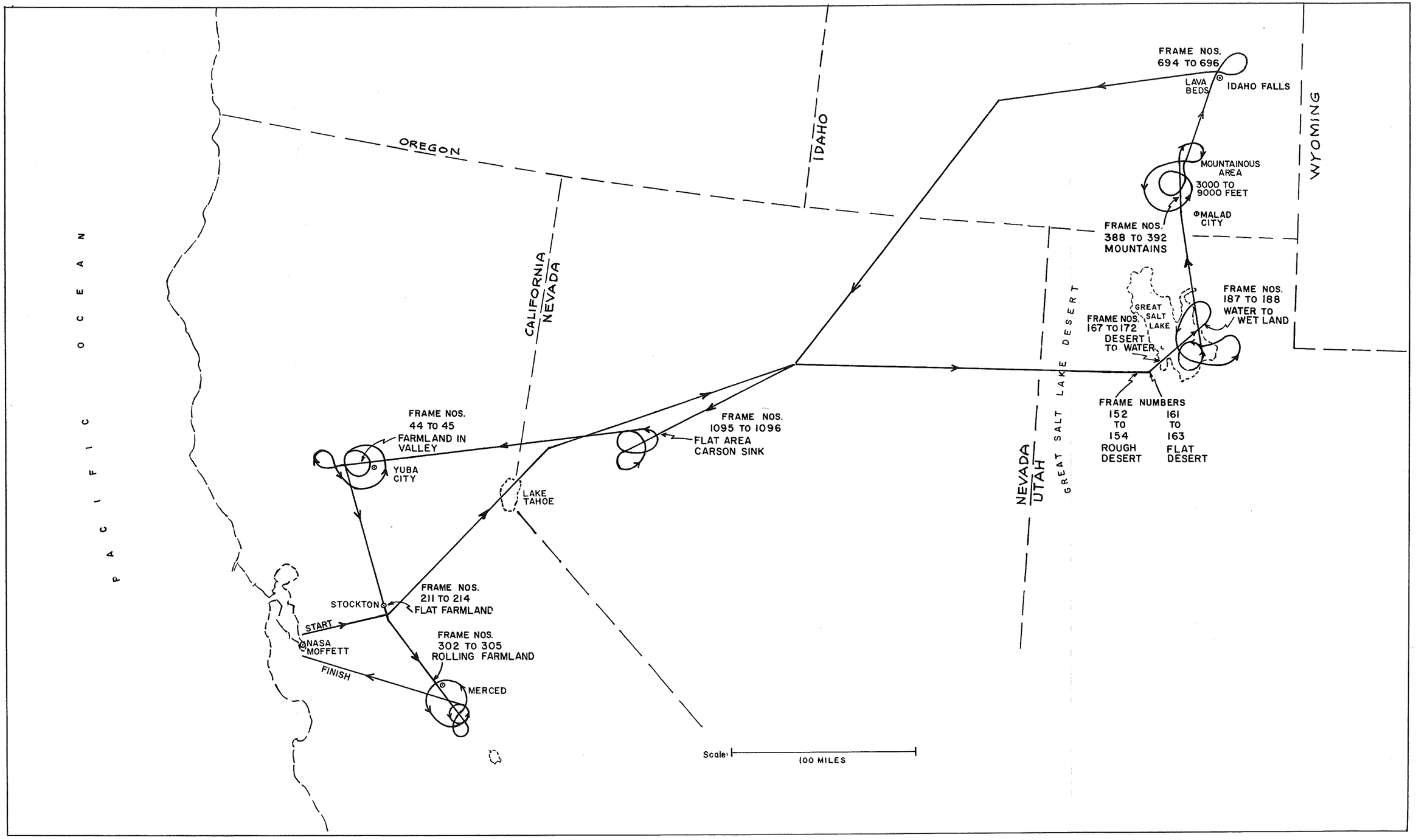

Fig. 17 Map of Flight Path for Measurement of Scattering Coefficients
October 11, 1967

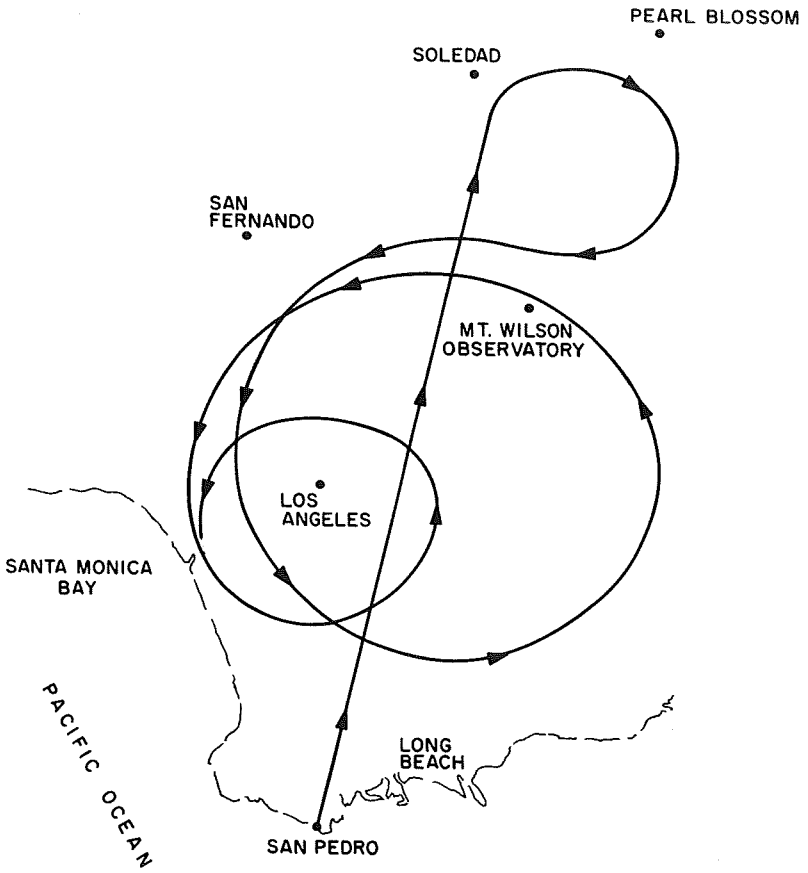

Fig. 18 Flight Track Over Los Angeles Area
October 12, 1967

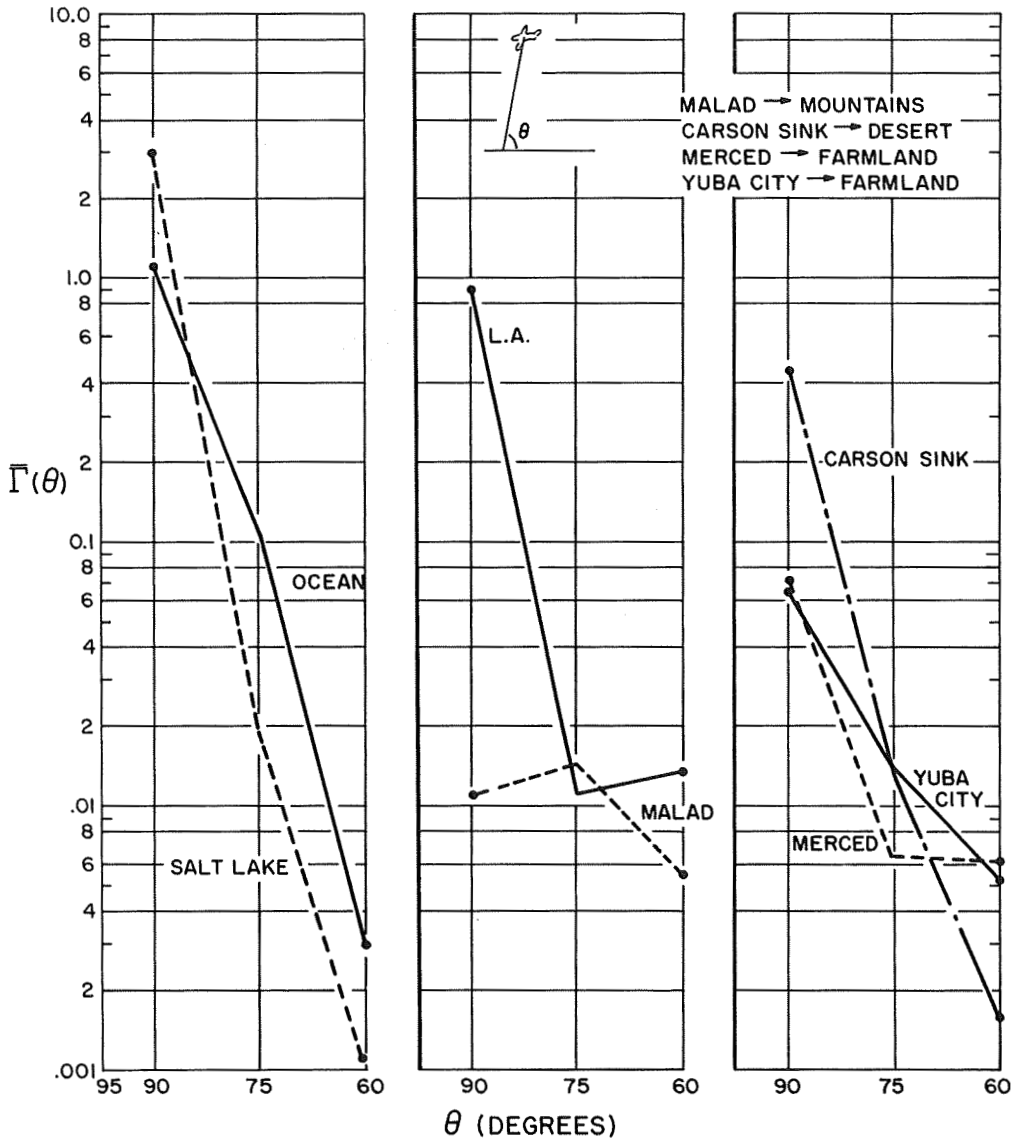

Fig. 19 Mean Value of Scattering Coefficient as a Function of the Angle of Incidence

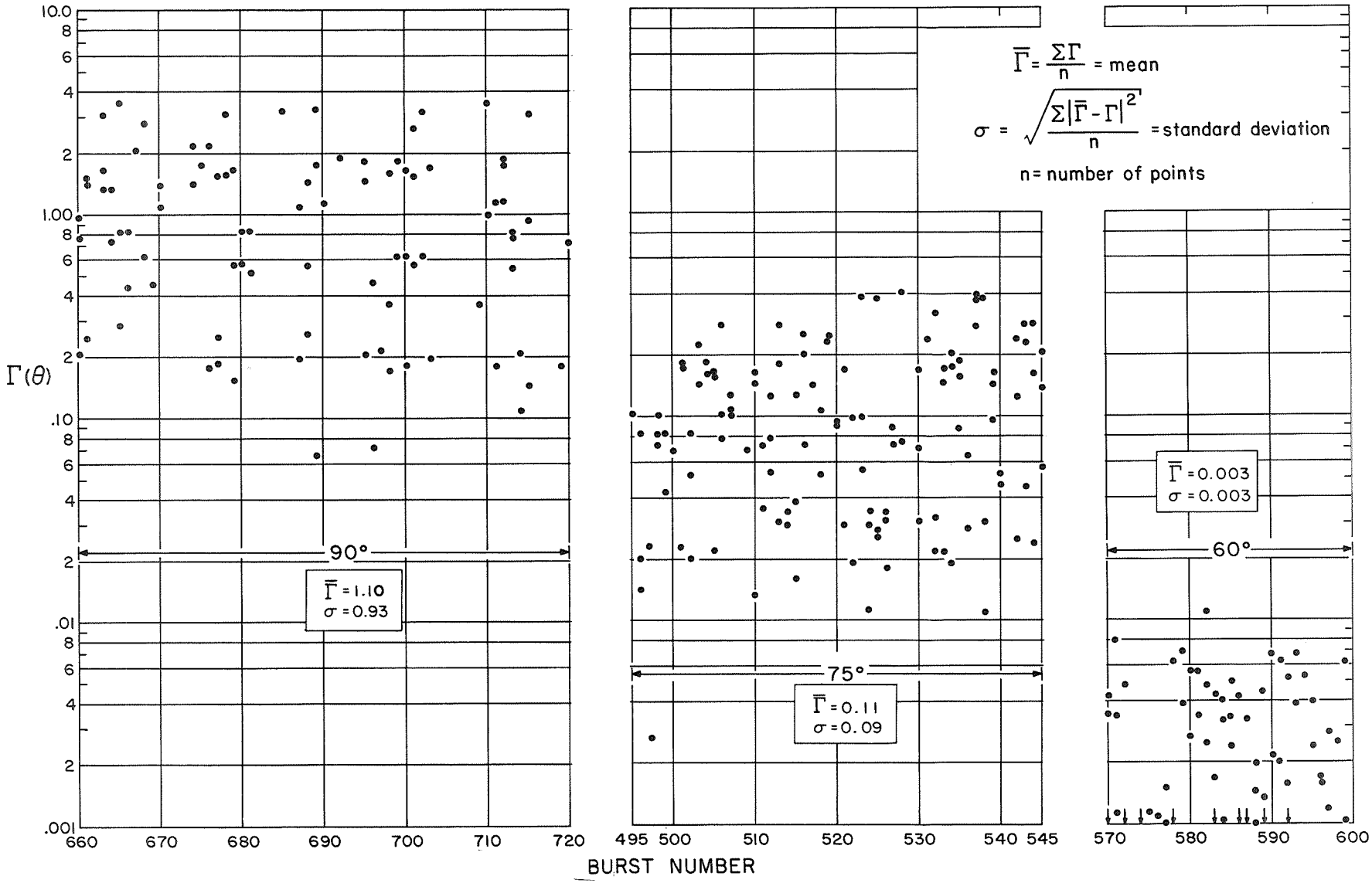

Fig. 20a Scattering Coefficient Measurements as a Function of Time
Pacific Ocean

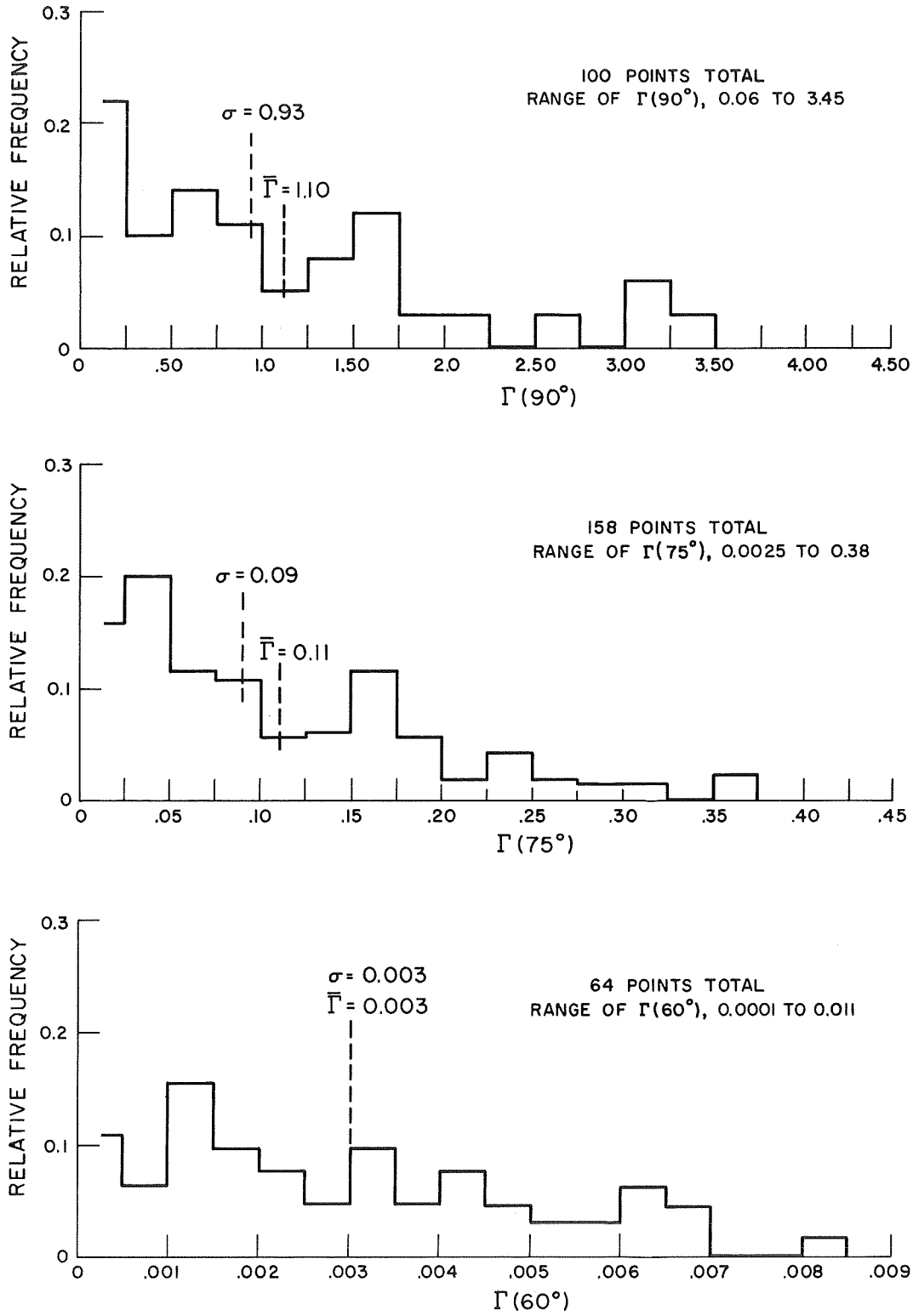

Fig. 20b Histograms of Scattering Coefficient Measurements
Pacific Ocean

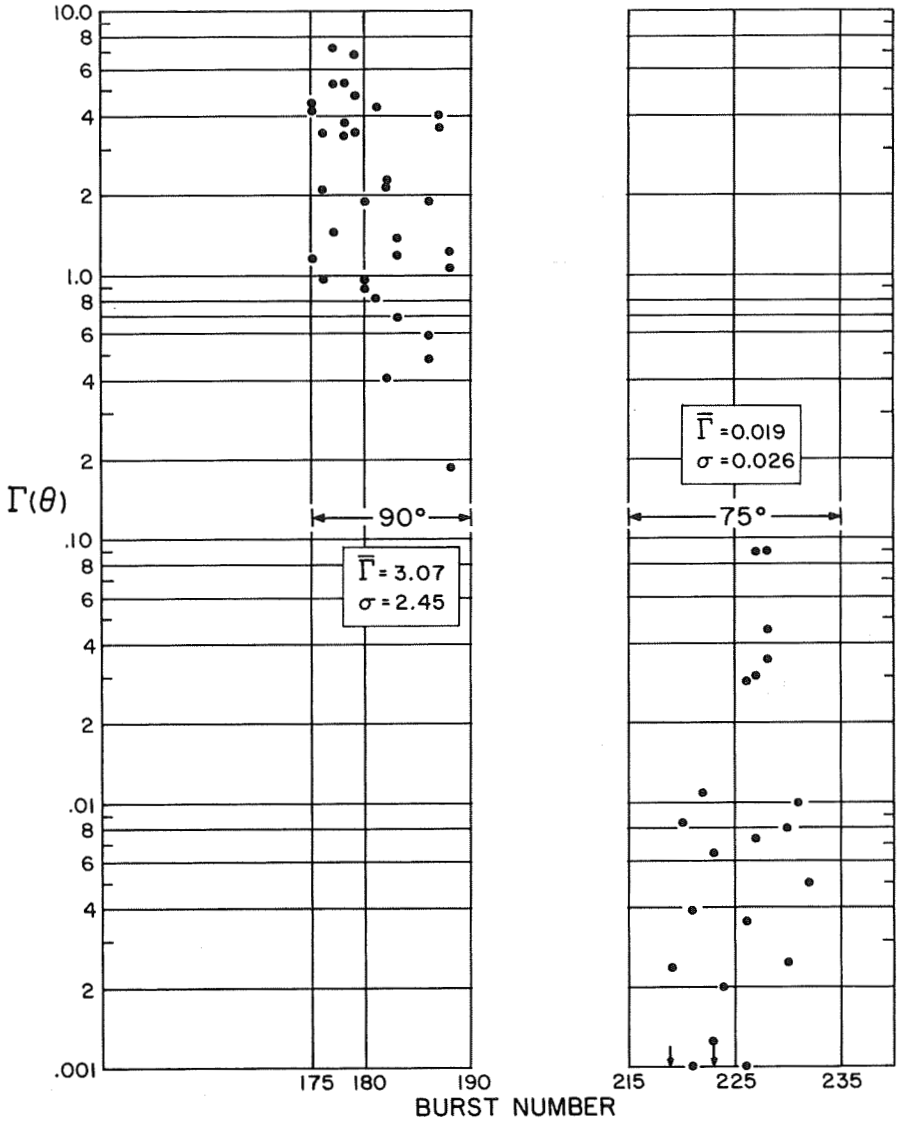

Fig. 21a Scattering Coefficient Measurements as a Function of Time
Great Salt Lake, Utah

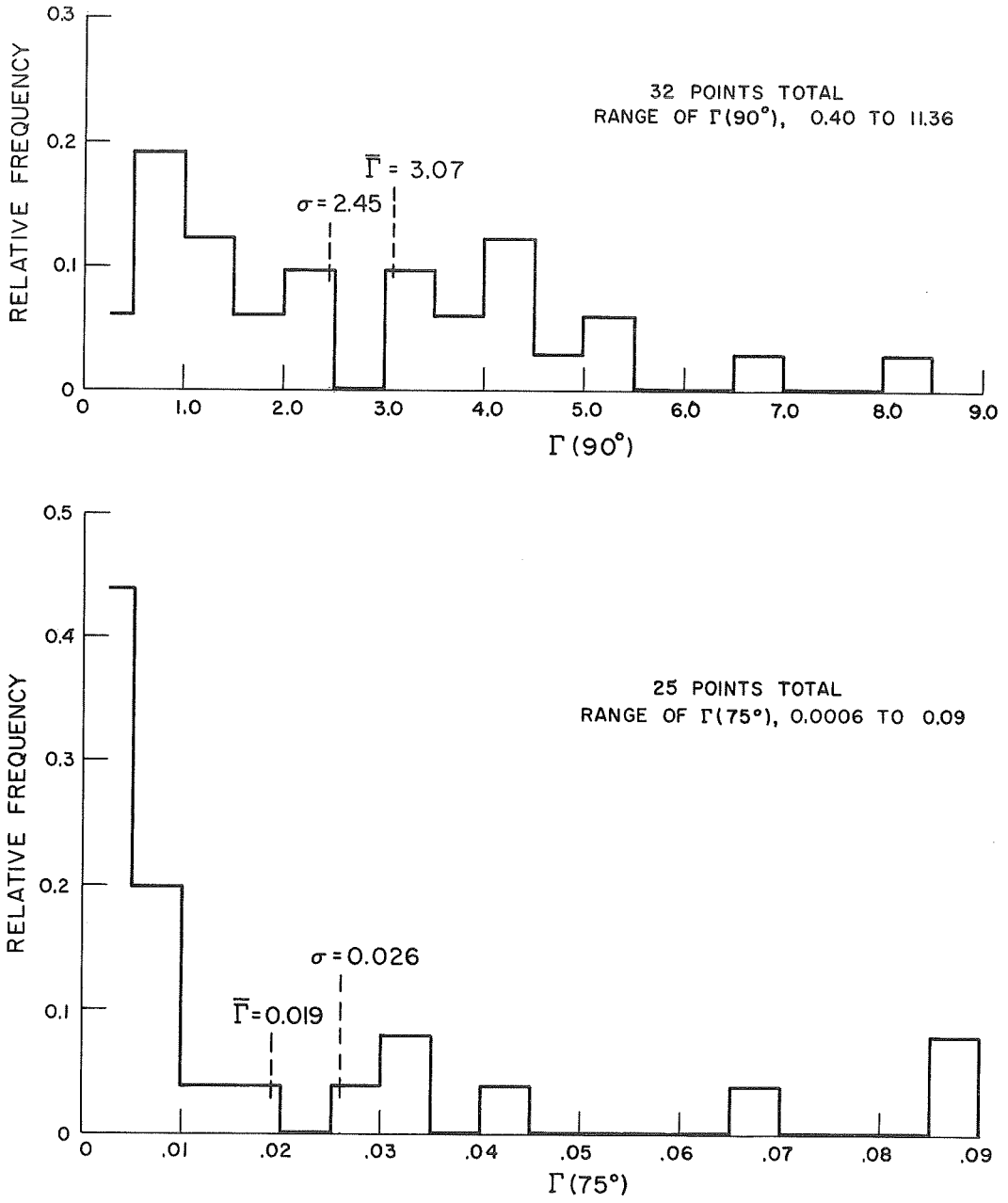

Fig. 21b Histograms of Scattering Coefficient Measurements
Great Salt Lake, Utah

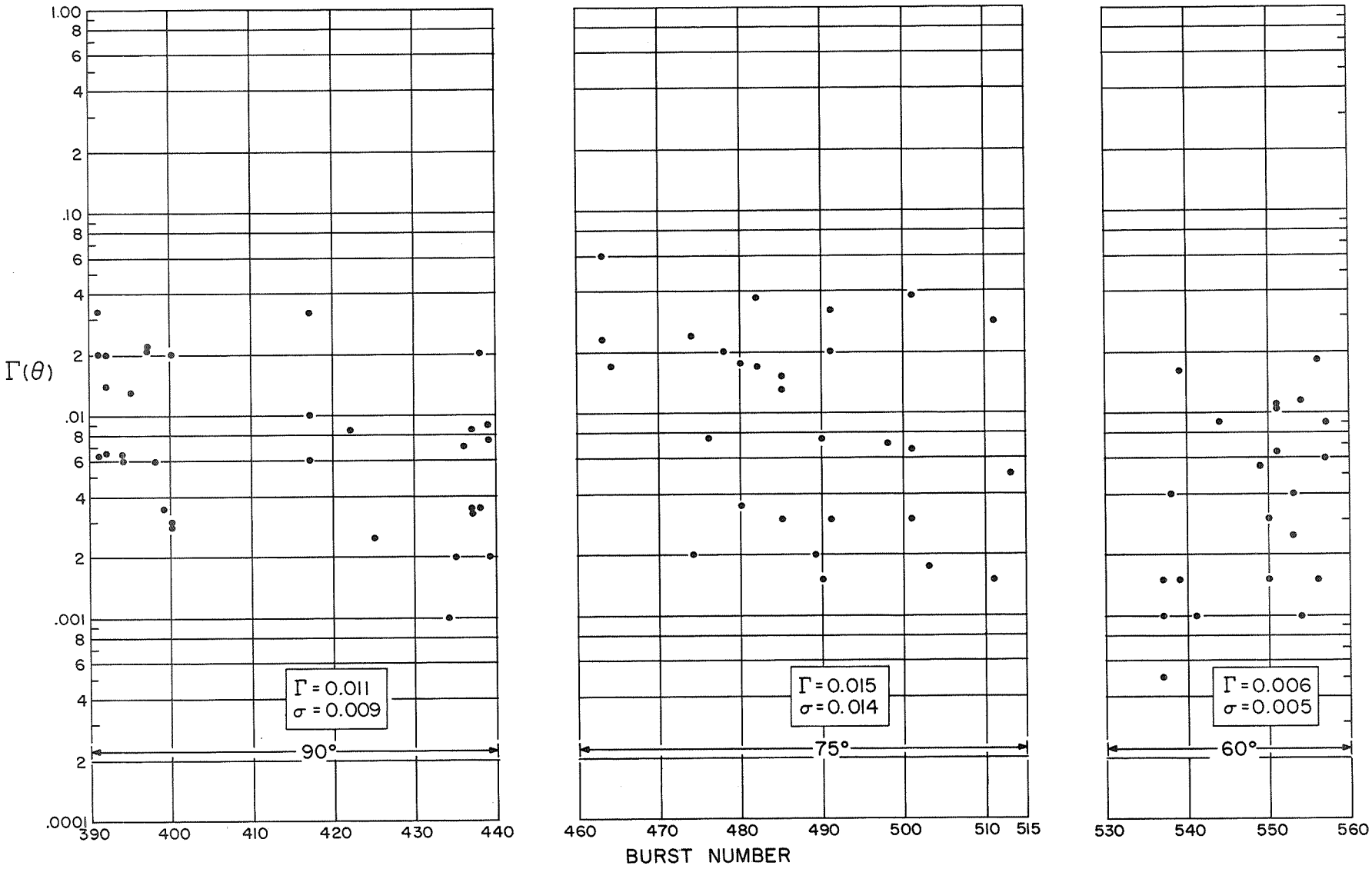

Fig. 22a Scattering Coefficient Measurements as a Function of Time
Malad, Idaho (Mountains)

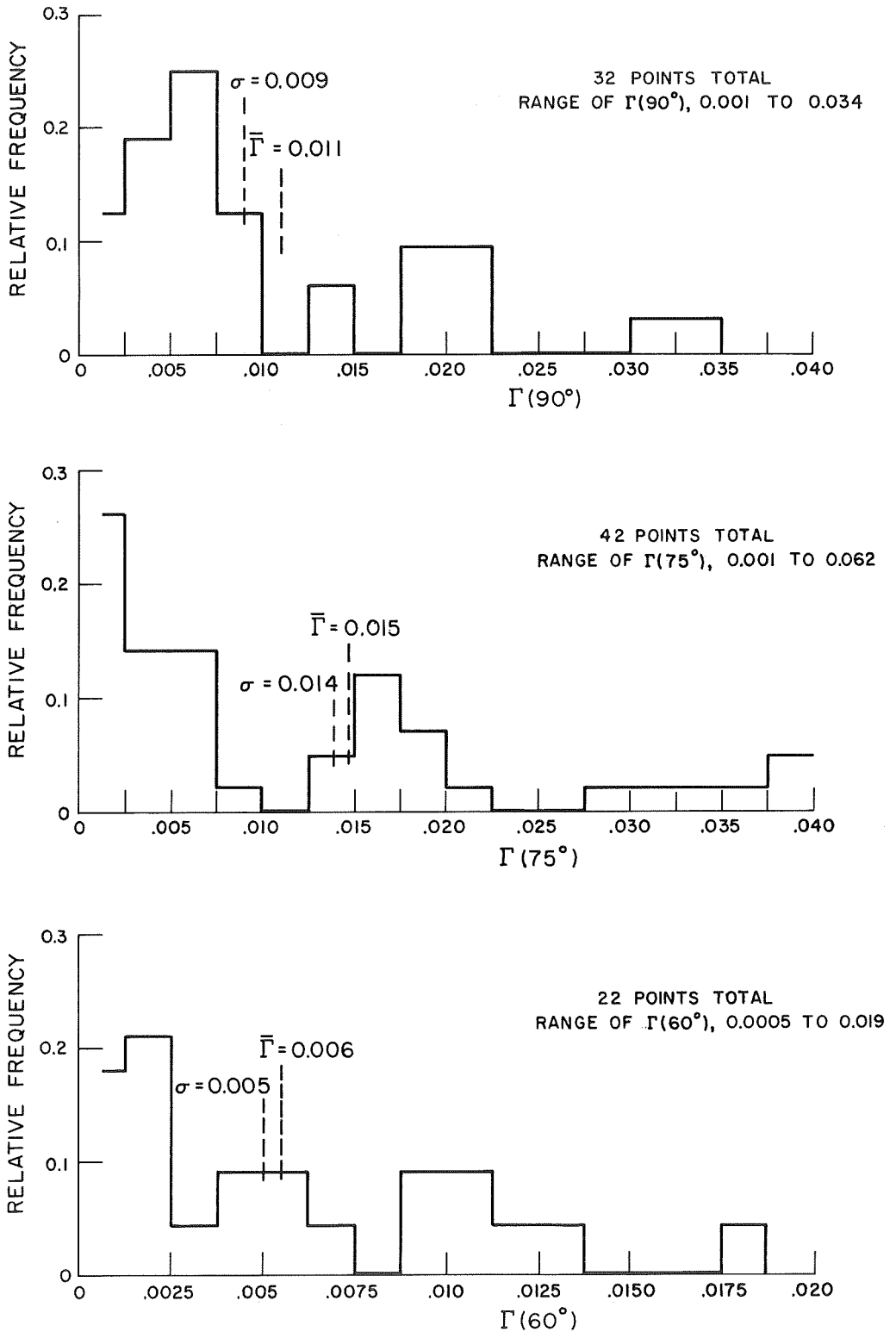

Fig. 22b Histograms of Scattering Coefficient Measurements
Malad, Idaho (Mountains)

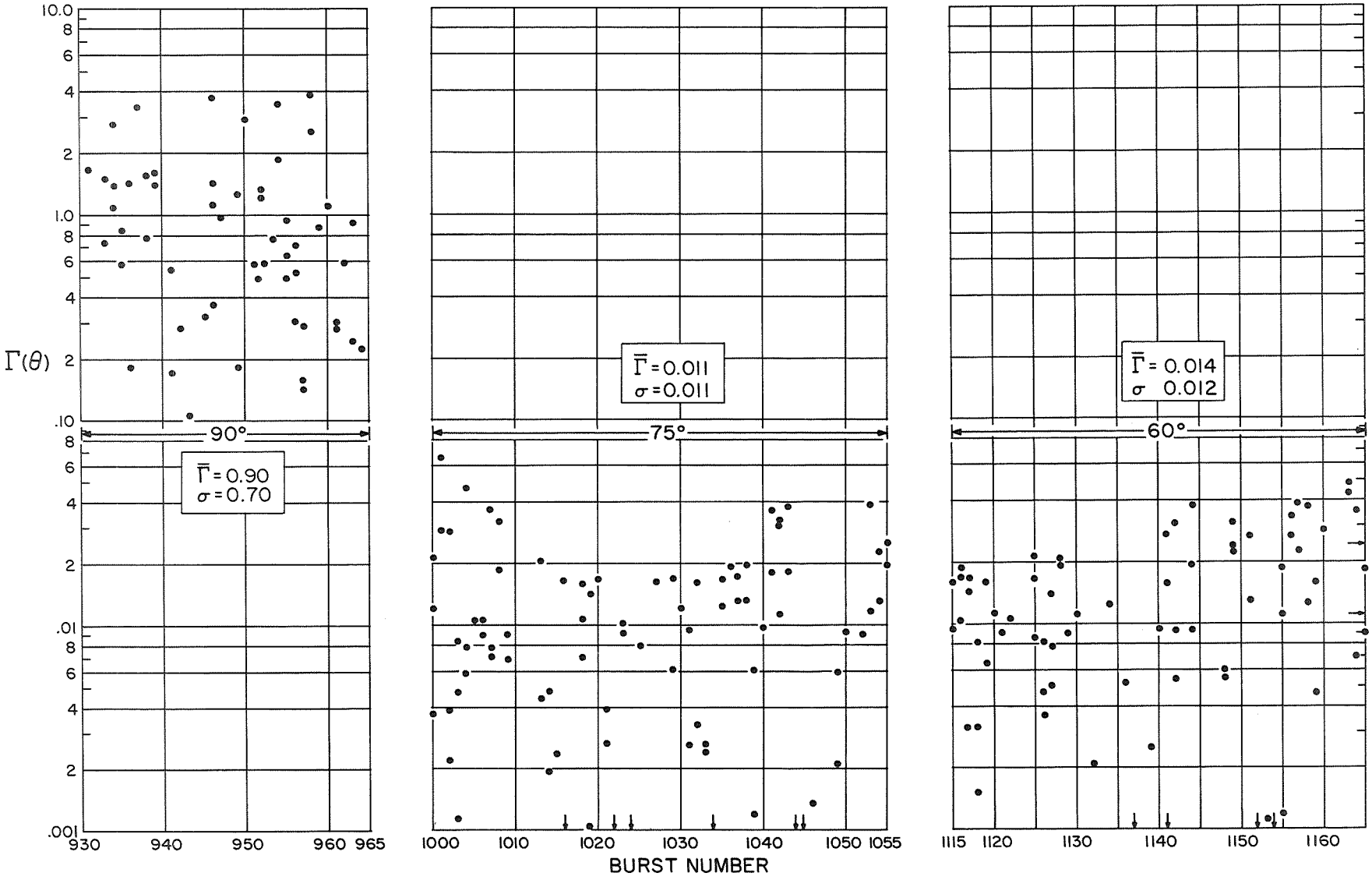

Fig. 23a Scattering Coefficient Measurements as a Function of Time
Los Angeles, California

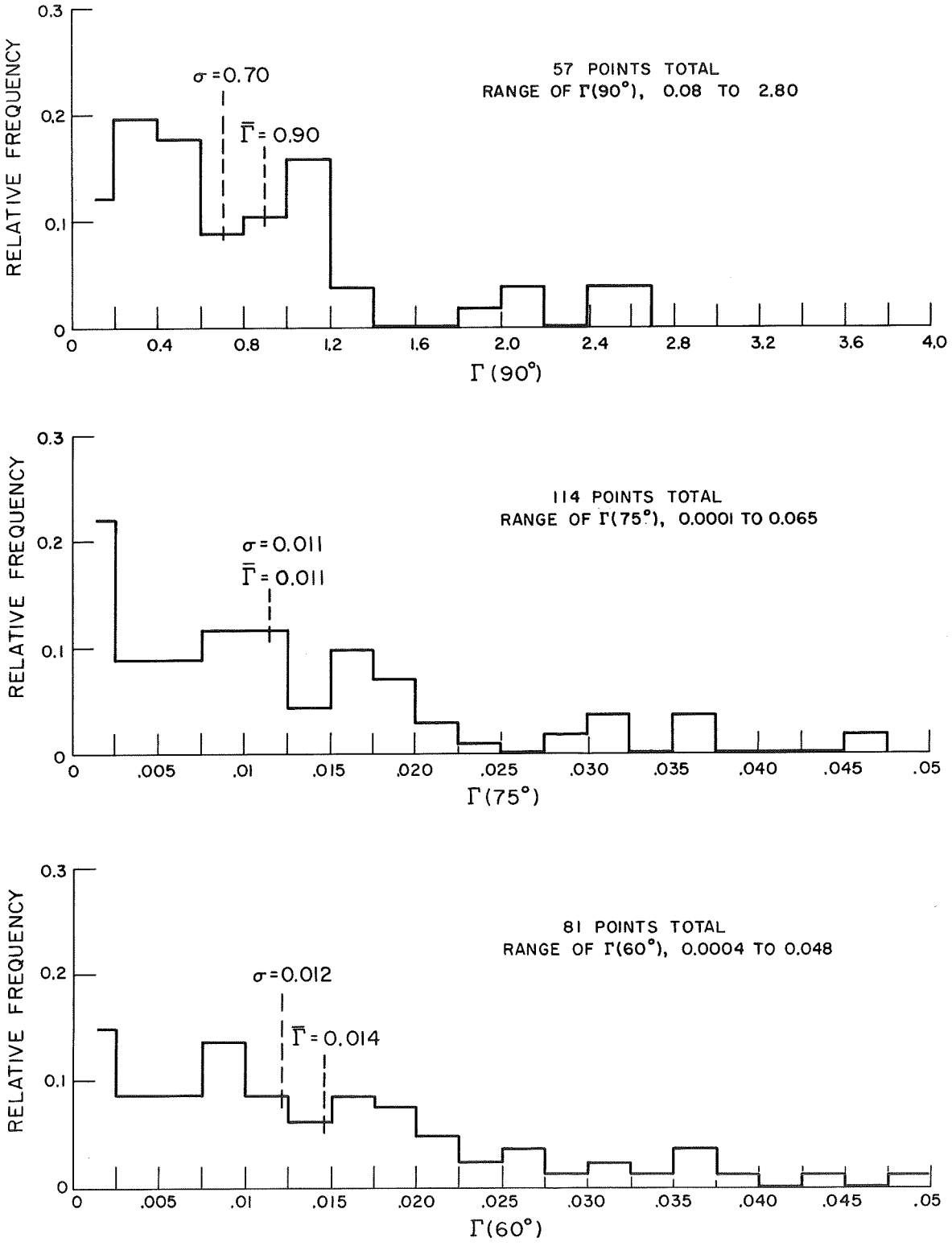

Fig. 23b Histograms of Scattering Coefficient Measurements
Los Angeles, California

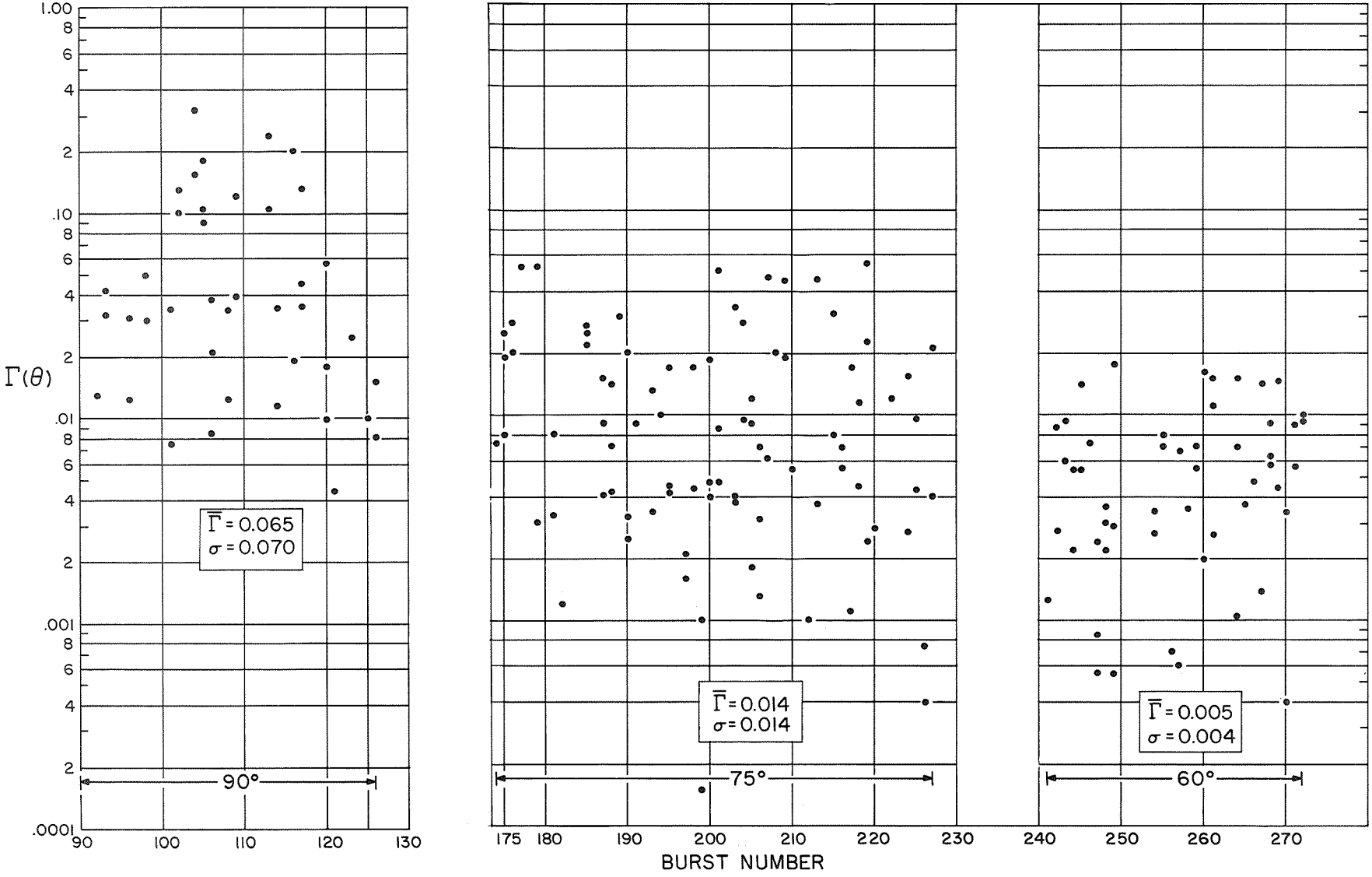

Fig. 24a Scattering Coefficient Measurements as a Function of Time
Yuba City, California (Farmland)

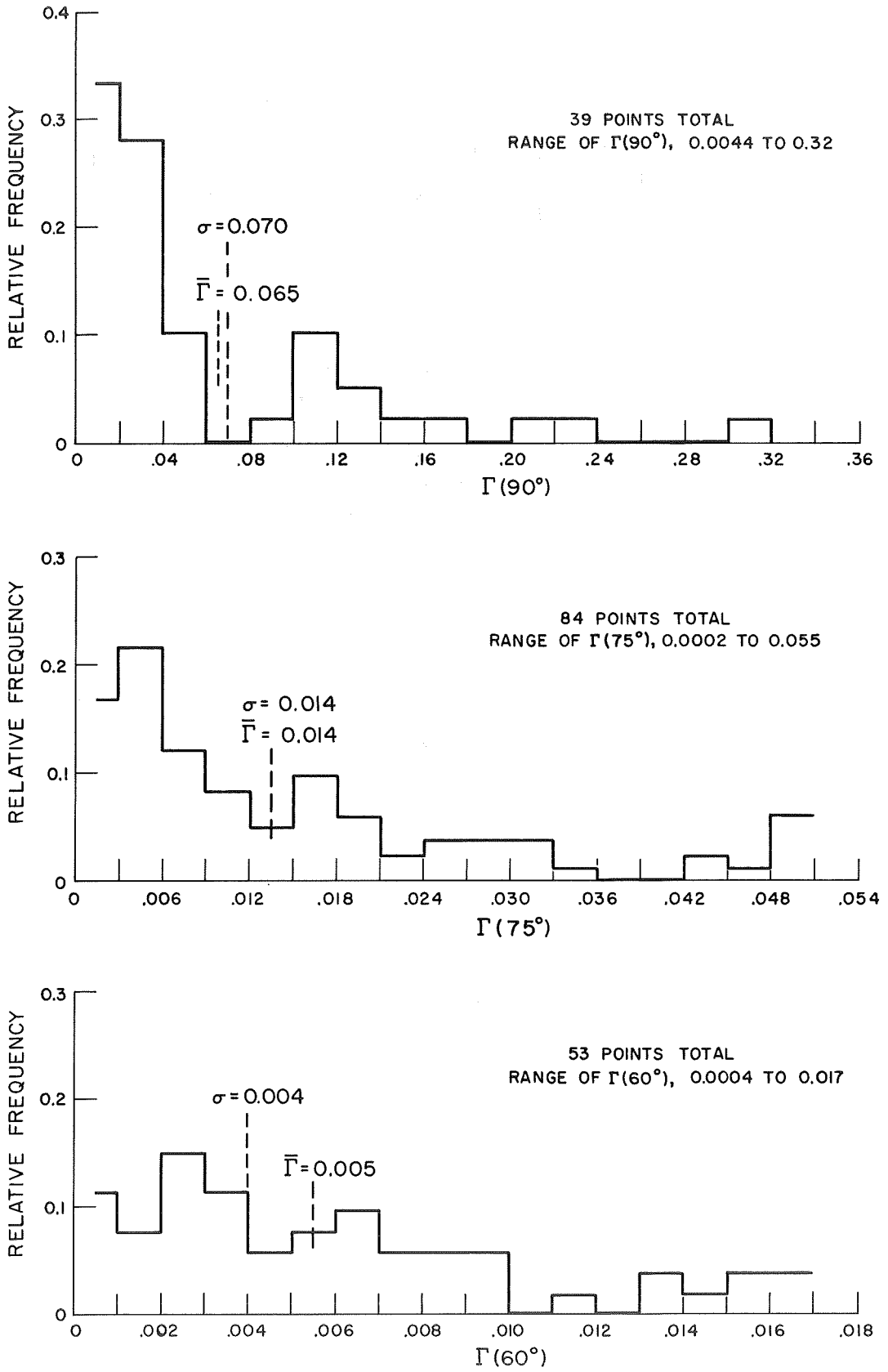

Fig. 24b Histograms of Scattering Coefficient Measurements
Yuba City, California (Farmland)

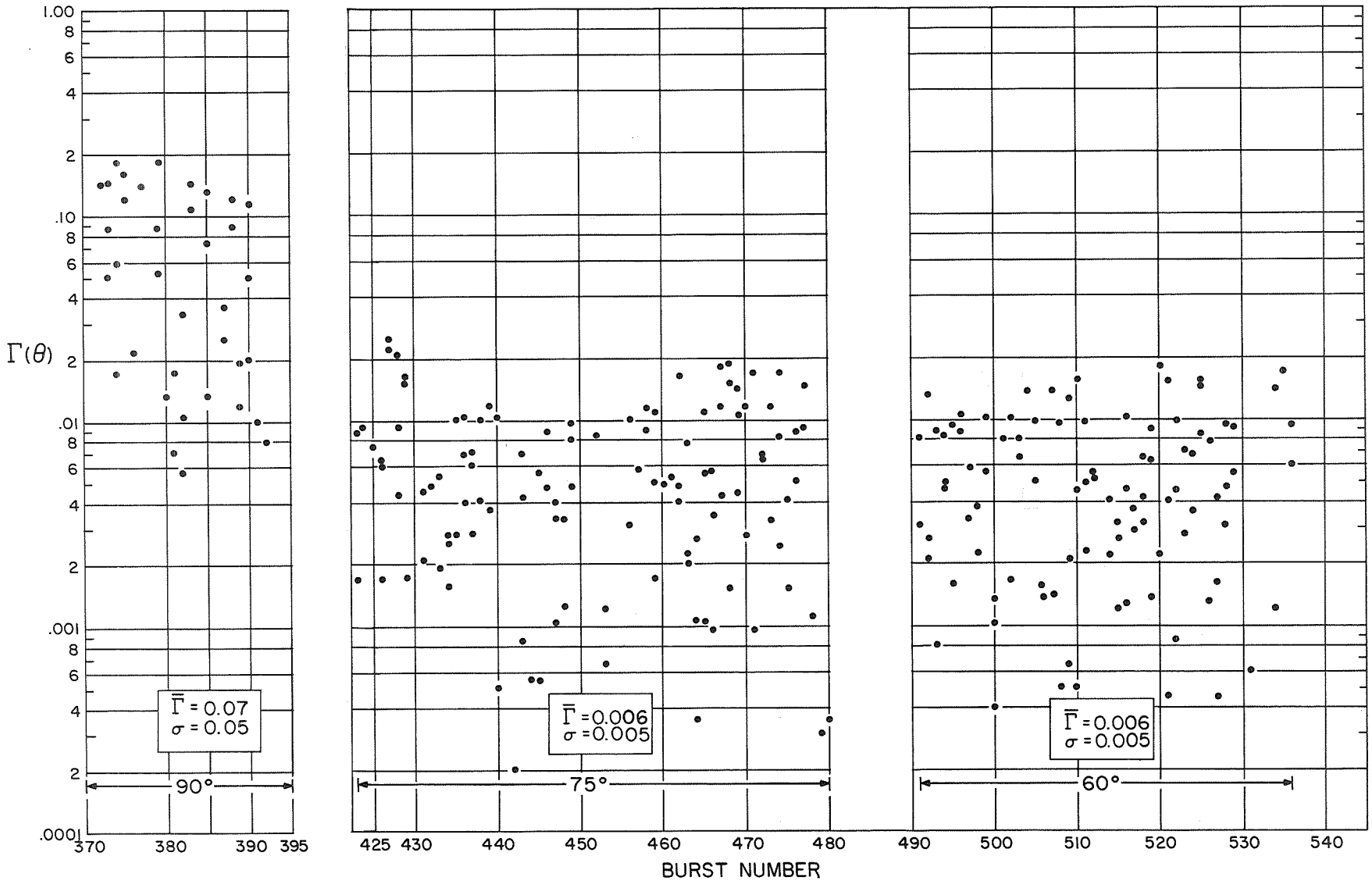

Fig. 25a Scattering Coefficient Measurements as a Function of Time
Merced, California (Rolling Farmland)

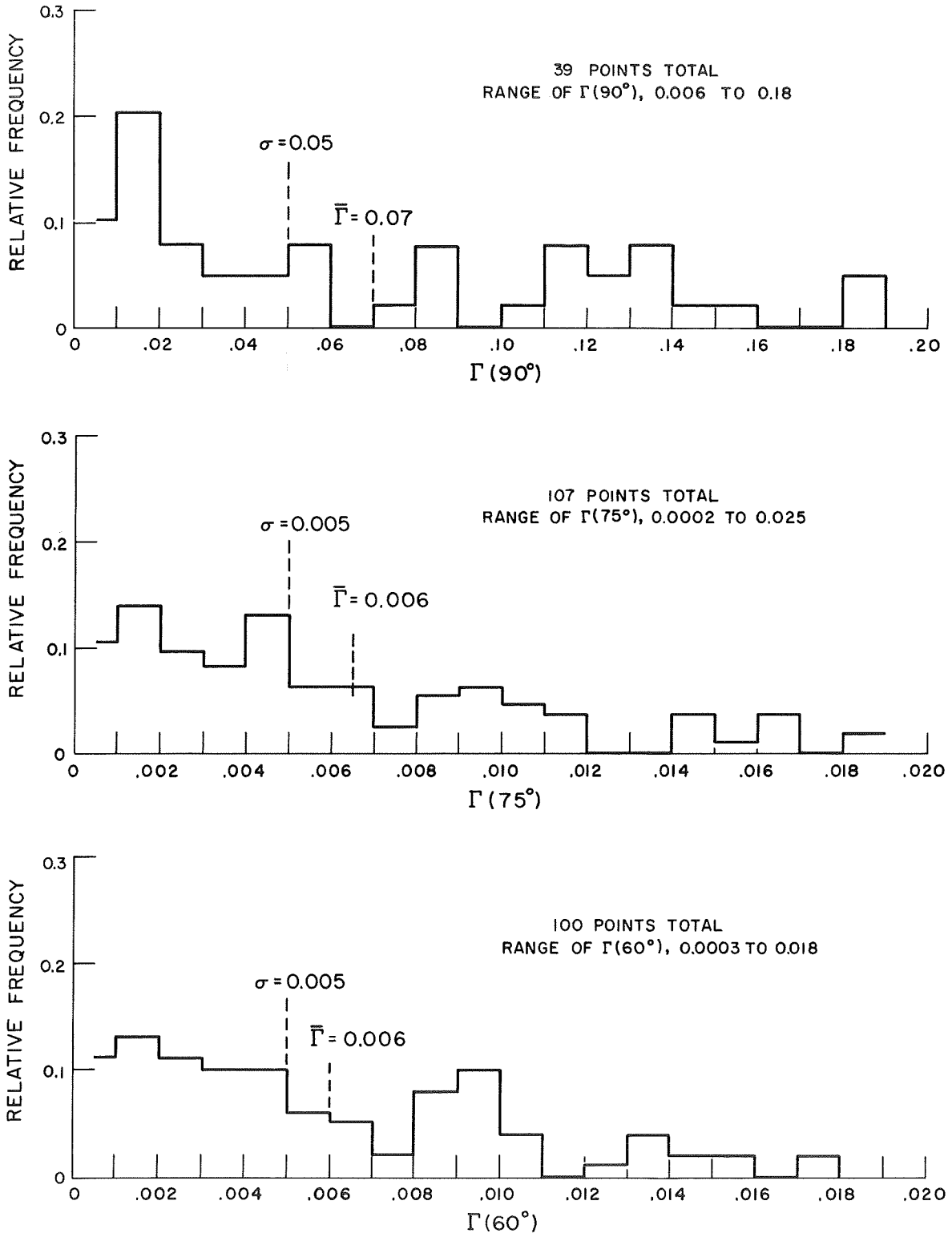

Fig. 25b Histograms of Scattering Coefficient Measurements
Merced, California (Rolling Farmland)

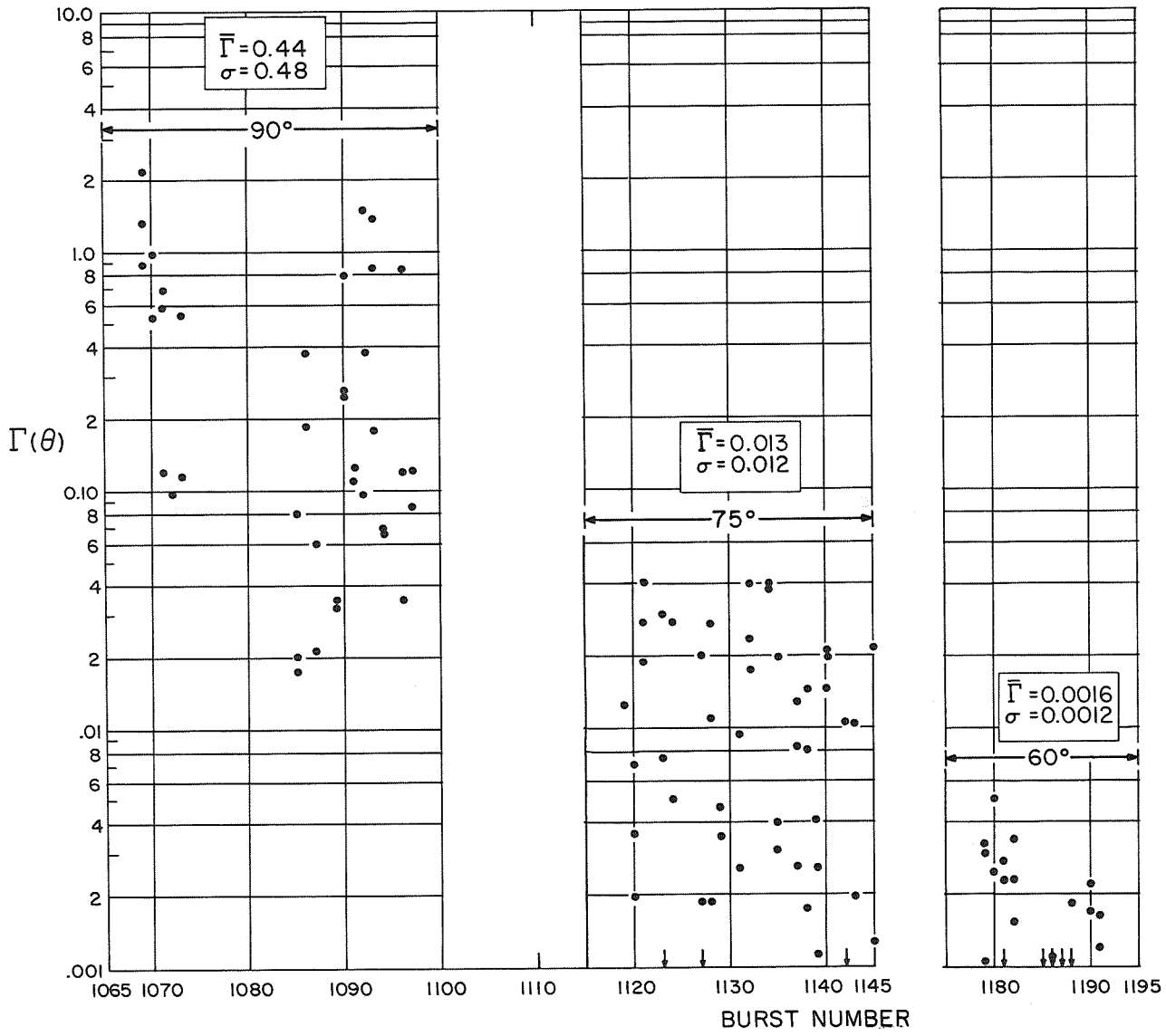

Fig. 26a Scattering Coefficient Measurements as a Function of Time
Carson Sink, Nevada (Desert Area)

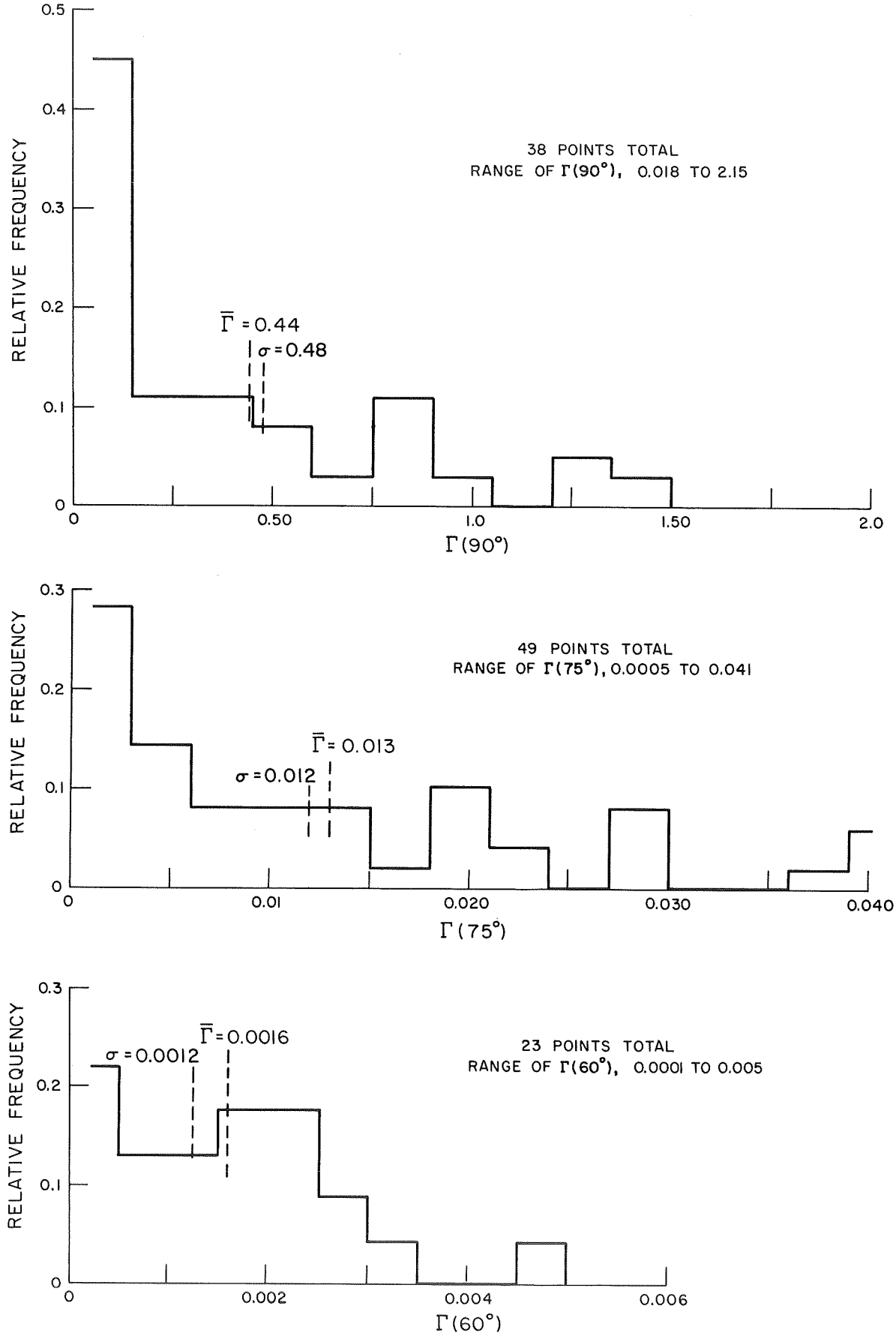

Fig. 26b Histograms of Scattering Coefficient Measurements
Carson Sink, Nevada (Desert Area)

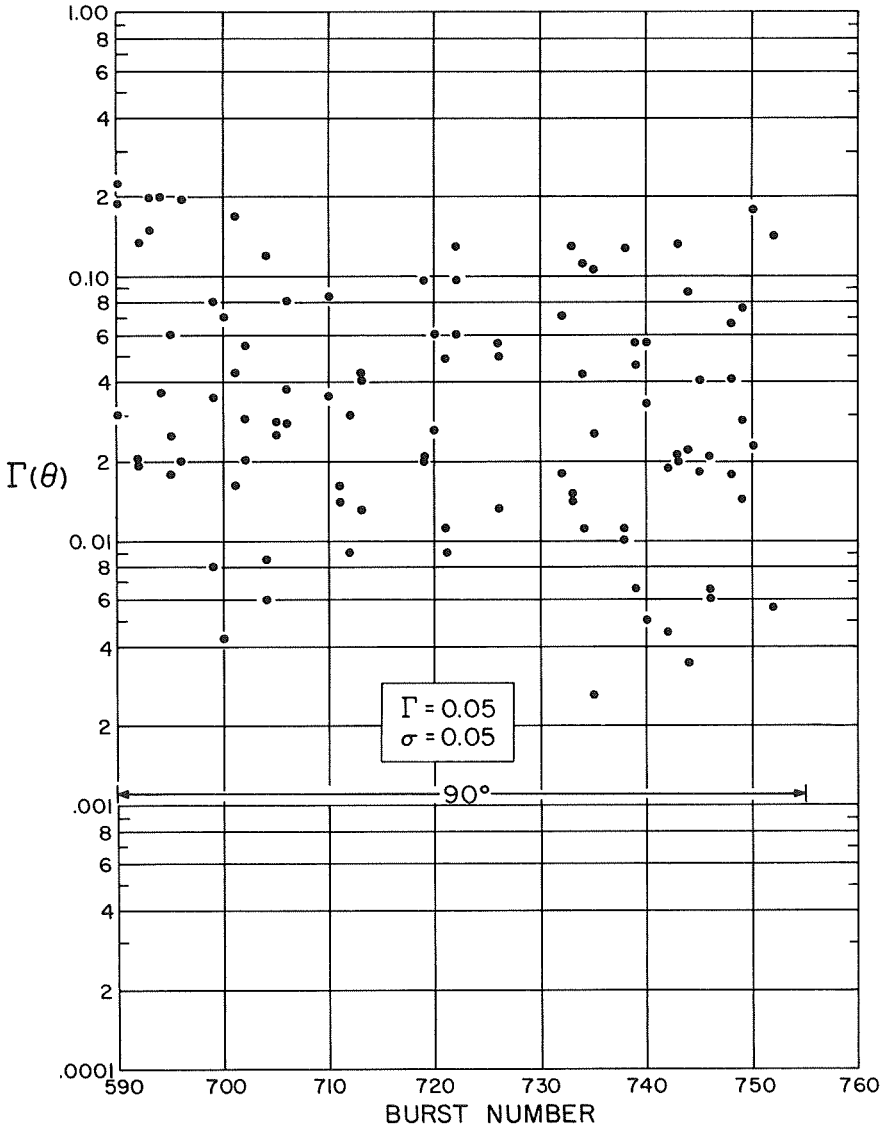

Fig. 27a Scattering Coefficient Measurements as a Function of Time
Idaho Falls, Idaho (Lava Beds)

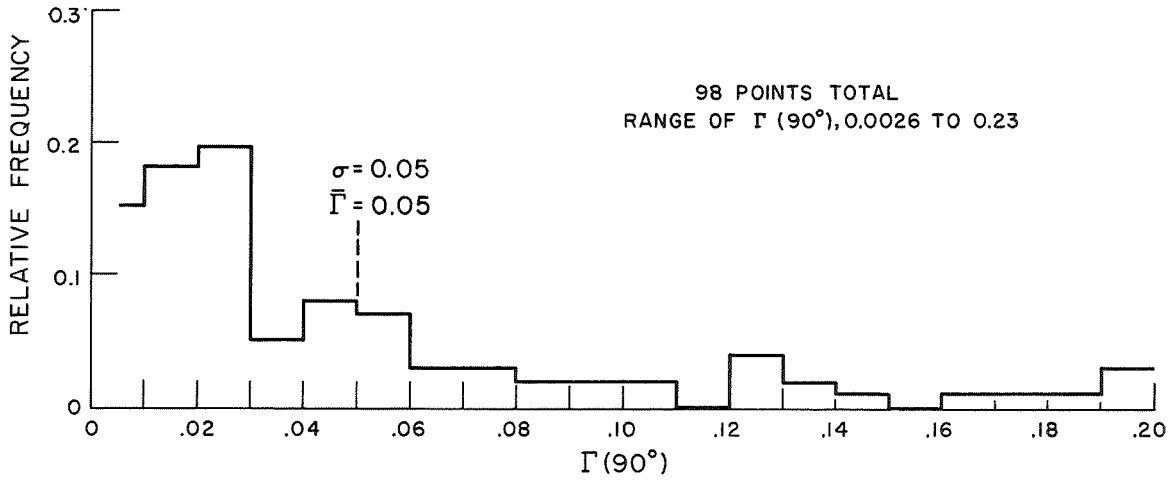

Fig. 27b Histogram of Scattering Coefficient Measurements
Idaho Falls, Idaho (Lava Beds)

in time of approximately eight seconds. The vertical scale is the scattering coefficient, each point representing one of the three pulses in the burst. When there are fewer than three points for a burst number it indicates that the data was unusable for one of the reasons stated previously. Listed on these graphs are the mean ($\overline{\Gamma}$) and the standard deviation (σ) of the scattering coefficient, calculated for each angle of incidence from the equations,

$$\overline{\Gamma} = \frac{\Sigma\Gamma}{n} \tag{5-1}$$

and

$$\sigma = \sqrt{\frac{\Sigma|\overline{\Gamma} - \Gamma|^2}{n}} \tag{5-2}$$

where n is the number of points.

The histograms show the same data as illustrated in Figs. 20a through 27a but in a different form. The horizontal scale is the scattering coefficient divided into an arbitrary number of steps and the vertical scale is the ratio of the number of measurements in the interval to the total number of measurements taken at the particular angle of incidence.

The curves plotted in Fig. 19 are a useful method of presenting the data since the scattering behavior of the different surfaces can be easily distinguished. Qualitatively, the shape of the curves is related to surface roughness, and the area under the curves (if data were over a full hemisphere) is indicative of surface composition. The value of the scattering coefficient at any angle of incidence depends on two factors: the surface composition, which determines the total amount of energy reflected from the surface in all directions, and surface roughness, which determines the relative amount of energy reflected into any direction. Performing measurements which would allow the effects of surface roughness and composition on the scattering coefficient to be separated present difficult experimental problems. Although the curves of Fig. 19 represent the mean value of backscattering measurements made with an antenna of 8^{o} beamwidth at only three different incidence angles, the curves are useful for making relative comparisons between the various target areas.

The seven target areas can be grouped roughly into three categories on the basis of the angular behavior of the scattering coefficient. Salt Lake, the Pacific Ocean and the desert area near Carson Sink are classed as quasi-specular scatterers; the mountains near Malad are diffuse scatters; and Los Angeles and the farmland near Yuba City and Merced are a combination of quasi-specular and diffuse. The two extremes of behavior are represented by Salt Lake and the mountains near Malad. The mean scattering coefficient from Salt Lake decreases 22 dB from normal incidence to 75^{o} and 13 dB further from 75^{o} to 60^{o}. The mean scattering coefficient at Malad actually increases 1 dB from normal incidence to 75^{o} and then decreases by 4 dB from 75^{o} to 60^{o}. It is easy to distinguish between relatively calm bodies of salt water and mountains by their angular scattering behavior. A more difficult comparison is that between scattering coefficients of the ocean and of the relatively flat desert area near Carson Sink. The scattering curves of Fig. 19 have approximately the same shape, that is, the scattering coefficient for the ocean decreases 10 dB in the first 15^{o} and 16 dB in the next 15^{o}. In comparison the desert area decreases 15 dB in the first 15^{o} and 9 dB in the next 15^{o}. The ocean was fairly rough with whitecaps visible on the day the measurements were made. Even so, the values of scattering coefficient were higher for the ocean than for the Carson Sink area. Furthermore, since the curves for the ocean and Carson Sink drop off quite rapidly, the area under the curves from just 90^{o} to 60^{o} (instead of over a hemisphere) is useful for comparing the total energy reflected from the two surfaces. Graphically integrating the area under the two curves gives the result that the area under the ocean curve is roughly four times the area under the Carson Sink curve. Presumably, this result is obtained because the salt water is a partial conductor even at 3 cm and thus reflects more energy than a nonconducting desert area.

The mean scattering coefficient curves for farmland near Yuba City and the rolling hills and farmland near Merced are quite similar, the values almost coinciding at 90^{o} and 60^{o}. This is a plausible result since the two areas are similar in surface roughness and compo-

sition. The Los Angeles area appears to be a diffuse scatterer except at normal incidence. The strong signals received at normal incidence are probably from flat areas such as rooftops or freeway surfaces.

The curves of Figs. 20a through 27a and 20b through 27b are intended to illustrate the time variation and distribution of the scattering coefficient. The points in Figs. 20a through 27a show the pulse-to-pulse variation during the 20-millisecond interval between successive pulses in a pulse burst. Also shown on the figures are calculated values of the mean and standard deviation of the scattering coefficient as defined in Eqs. 5-1 and 5-2. The plane moved approximately 15 feet during the 20-millisecond time interval between pulses. Since the return signal varied considerably from pulse to pulse by as much as 16 dB, the conclusion is reached that 15 feet is greater than the decorrelation distance. Presumably, if the pulses were spaced successively closer together, some point would be reached where the pulse-to-pulse variation would be quite small. Apparently the surface roughness would have an affect on the required pulse spacing, that is, a truly smooth surface would give the same return from pulse to pulse regardless of the spacing. There is a possibility that an indication of surface roughness would result from measurements of decorrelation time. The experiment performed had a fixed pulse spacing so there was no data gathered on pulses spaced closer than 20 milliseconds.

The histograms present the amplitude distribution of the scattering coefficient in a convenient form. The shape of the histograms suggests a Rayleigh distribution, but the paucity of data for some of the target areas does not permit a firm conclusion to be reached. The absence of data in some of the histogram intervals is due to an insufficient number of measurements. Most of the histograms resemble Rayleigh distributions in that the greatest number of points occur in the first interval, and the mean and standard deviation are approximately equal. When the data are Rayleigh-distributed it indicates that the received signal is the sum of a large number of small signals of almost constant amplitude and random phase. Some of the histograms, however, do have the largest number of points in the second interval, for example,

the histograms for the ocean at 75^{o} and 60^{o}. This indicates that the scattered signal is the sum of a constant signal plus a large number of small random signals.

The flight-test experiment was, on the whole, successful. A productive amount of data on the X-band backscattering properties from a variety of surfaces were recorded. Analysis of these data leads to the conclusion that gross surface features can be deduced by measurements of this kind. In particular, the mean scattering coefficient, when measured as a function of angle of incidence of the impinging radiation, has proved to be an effective method for interpreting the data.

The electromagnetic-radiation-measurement equipment used in the system, in general, performed satisfactorily. However, results indicate that certain performance improvements can be attained. Specifically, the following modifications should be made:

1. Redesign of the receiver automatic gain control system to accommodate the large pulse-to-pulse amplitude variations in the echo signals.

2. Increase the system duty factor to allow the gathering of more data in less flight time.

3. The capability to alter the transmitted waveform during flight to observe the effects of surface properties on the decorrelation time of the scattering coefficient.

Consideration has been given to methods of gathering additional information for the purpose of identifying surface features. One possibility is the use of a radar and radiometer operated as a dual-mode measurement instrument. The instrument, a tentative design for which is presented in the next chapter, would operate in the radar mode to gather backscatter measurements. In the radiometer mode, radiant-temperature measurements would be made of the surface of interest. Radiometer measurements would be made during radar off-time and would utilize the radar-receiver circuitry.

VI RADAR-RADIOMETER DUAL-MODE CONCEPT

The measuring instrument discussed so far in this report operates in a pulsed-radar mode and is designed to transmit microwave energy in bursts and then to measure the amount of energy reflected from a surface. The scattering coefficient is calculated from measurements made by the radar and this information allows gross features of the surface to be inferred.

The experiment concept and the need to budget prime power requires that the radar-measuring instrument be in its ON or operating mode at approximately 10 percent of its in-flight time. The concept of a dual-mode or radar-radiometer instrument utilizes the receiver circuitry during the radar-instrument OFF-time, as shown in Fig. 28.

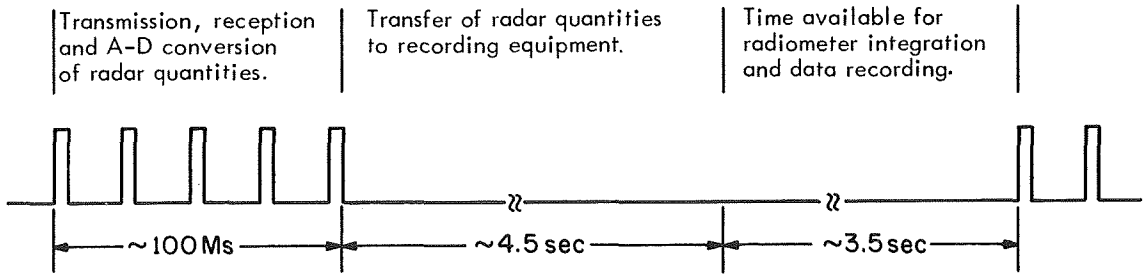

Fig. 28 Combined Radar-Radiometer Format

It is estimated that the dual-mode instrument would increase power consumption and total spacecraft instrument weight about 10 percent over that of the present radar instrument. It has the advantage of permitting radiometric data on surface patches to be gathered during quiescent intervals of the radar.

A. BASIS FOR RADIOMETER CONFIGURATION

Electromagnetic waves emanate from all objects in the physical universe that are at a thermal temperature above absolute zero. The objective is to use the radiometer part of the combined instrument to measure the radiant energy from the surface of interest at the frequency of radar operation (9.72 GHz). Thus, the radiometer is concerned with the measurement of microwave radiation emanating from the planetary

surface rather than with measurements of signals arising from back-scattering; the radiometric measurements resemble optical information more nearly than they do data from a mapping radar.

In practice, the reflections detected by the radiometer are similar to the thermal and shot noise in the receiver. It follows that the receiver must detect a change in the output noise power when a small amount of signal noise is present at the antenna terminals.

B. CONCEPTUAL CONFIGURATION

The minimum detectable signal of a radiometer is determined by (1) the gain fluctuation of the receiver and (2) by the statistical fluctuations in a noise-like waveform. These two effects combine to produce a fluctuating receiver output in the absence of a signal. The method that is commonly used to reduce the effects of (1) is to modulate the signal at some frequency at which the level of this effect is negligible. The signal level is then determined by using a coherent detector driven synchronously at the modulation frequency. This type of radiometer was originally described by R. H. Dicke* and employed a 30-cps modulation of the signal by mechanically switching the receiver input between the antenna and resistive load at room temperature. Thus the thermal noise present at the antenna was compared with the thermal noise of the resistor. The modulation pattern can be represented by a square wave where one half-period contains signal information followed by another half-period containing comparison information.

A block diagram of a possible configuration of a dual mode instrument is shown in Fig. 29. A goal of the design is to use techniques and devices that will result in light-weight and low-power consumption.

---

*Dicke, R. H., "The Measurement of Thermal Radiation at Microwave Frequencies," The Review of Scientific Instruments, Vol. 17, No. 7, July 1946.

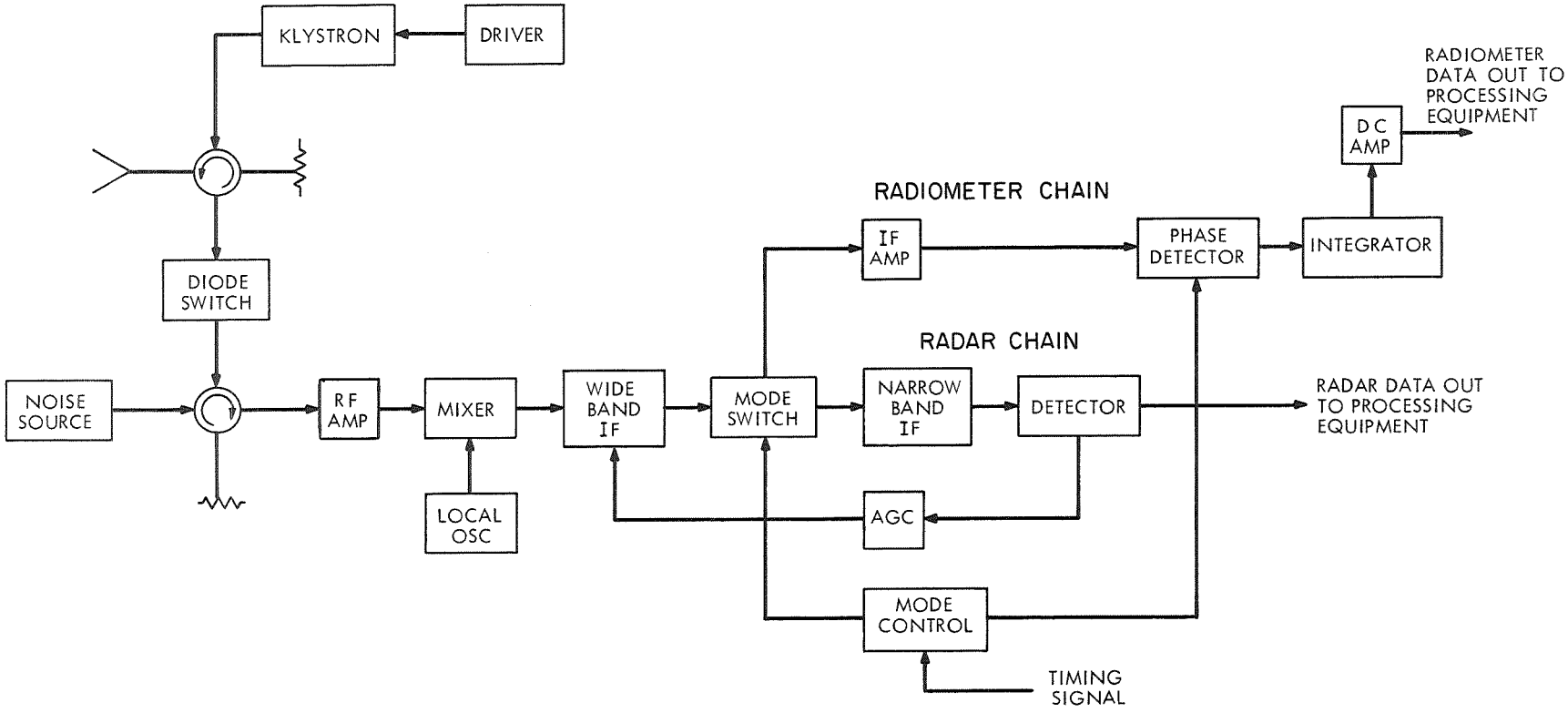

Fig. 29 Simplified Block Diagram of Radar-Radiometer Instrument

C. PROGRAM RESULTS

Work was initiated on the dual-mode measuring instrument but could not be completed during the remaining time period of the grant. The r-f switching between the noise source and the antenna was carried out through use of a circulator and a solid-state diode switch. This method consumes less power than does a ferrite switch which is often employed in this application.

The design and construction of a noise source was also initiated. Noise temperature was centered at 600°K and a 2°K temperature resolution was established. A unique characteristic was the method of contructing a microstrip-to-waveguide transition having the lowest possible mismatch. A VSWR of the order of 1.03 was obtained.

Sufficient work was undertaken to validate the belief that a dual-mode instrument will be simpler, more compact, and have higher efficiency than two separate instruments.

VII PUBLICATIONS OF THE PROJECT

REPORTS AND MEMORANDA

1. Reintjes, J.F., et al., "X-Band Scattering Measurements of Earth Surfaces from an Aircraft," Electronic Systems Laboratory Report ESL-R-370, Massachusetts Institute of Technology, Cambridge, Massachusetts, September 1968.

2. Reintjes, J.F., et al., "Flight Tests of a Radar Scattering-Coefficient Measuring Instrument," Electronic Systems Laboratory Report ESL-R-340, Massachusetts Institute of Technology, Cambridge, Massachusetts, February 1968.

3. Bosco, J.A. and Roberge, J.K., "High Efficiency D-C to D-C Converter-Regulators," Electronic Systems Laboratory Report ESL-R-288, Massachusetts Institute of Technology, Cambridge, Massachusetts,November 1966.

4. Arnn, E.L., "R-F Simulation for Long-Pulse Radar," Electronic Systems Laboratory Technical Memorandum ESL-TM-273, Massachusetts Institute of Technology, Cambridge, Massachusetts, June 1966.

5. Osman, M.S., "A Mechanism for 1/f Noise of Thin Evaporated Metal Films," Electronic Systems Laboratory Report ESL-R-149, Massachusetts Institute of Technology, Cambridge, Massachusetts, September 1962.

6. Roberge, J.K., "Design of Spacecraft Radar Systems for Investigation of the Planet Venus," Master of Science Thesis, Electrical Engineering Department, Massachusetts Institute of Technology, Cambridge, Massachusetts, June 1962.

7. Dertouzos, M.L. and Roberge, J.K., "Reaction-Wheel Attitude Control of Space Vehicles," Electronic Systems Laboratory Technical Memorandum ESL-TM-135, Massachusetts Institute of Technology, Cambridge, Massachusetts, March 1962.

8. Dertouzos, M.L. and Bosco, J.A., "Design of a Radar System for Measuring the Electromagnetic-Reflection Characteristics of the Earth's Surface from a Satellite," Electronic Systems Laboratory Internal Memo 9461-M-5, Massachusetts Institute of Technology, Cambridge, Massachusetts,

TECHNICAL PAPERS

9. Reintjes, J.F., "Reflection Coefficients of Planetary Surfaces from Unmanned Spacecraft," presented at the Second IFAC Symposium on Control in Space, Vienna, Austria, September 1967. Published in Proceedings of the Symposium, Instrument Society of America, September 1967.

10. Roberge, J.K., "A Low-Power High Efficiency DC to DC Converter," presented at the Solid State Circuits Conference, University of Pennsylvania, February 1965. Published in the Digest of Technical Papers, pp. 72-73.

11. Roberge, J.K., and Sarles, R.W., "Low-Power Fast Pulse Circuit Techniques in the MIT Gamma-Ray Telescope," presented at the Conference on Nuclear Instrumentation, Philadelphia, Pennsylvania, November 1964. Published in I.E.E.E. Transactions on Nuclear Science, February 1965.

12. Dertouzos, M.L., "An Approach to Threshold Element Synthesis," I.E.E.E. Transactions on Electronic Computers, October 1964.

13. Dertouzos, M.L. and Roberge, J.K., "High Capacity Reaction-Wheel Attitude Control," Joint Automatic Control Conference, Minneapolis, Minnesota, June 1963, pp. 428-436.

14. Advani, G.T., Gottling, J.G. and Osman, M.S., "Thin Film Triode Research," Letter, Proc. I.R.E., Vol. 50, No. 6, June 1962, pp. 1530-1531.

STATUS REPORTS

15. J.F. Reintjes and Staff, "Venus Radar Systems Investigations," Semiannual Status Report for the period May 1, 1963 - April 30, 1964, ESL-SR-199, dated May 1964.

16. J.F. Reintjes and Staff, "Venus Radar Systems Investigations," Semiannual Status Report for the period October 1,1962 - April, 30,1963, ESL-SR-178, dated May 1963.

17. J.F. Reintjes and Staff, "Venus Radar Systems Investigations," Semiannual Status Report for the period April 1, 1962 - September 30, 1962, ESL-SR-157, dated November 1962.

THESES

Doctor of Science

18. Roberge, James K., "Gated Amplifiers for Data Processing in Space," August 1966.

Master of Science

19. Haase, Wayne C., "A Novel Analog Multiplier," June 1967.

20. Sadler, William G., "A Flush-Mounted X-Band Horn-Lens Antenna," June 1966.

21. Arnn, Edward L., Jr., "A Special-Purpose X-Band Radar-Target Simulator," September 1965.

22. Cobb, D., "Differential Operational Amplifier Using Field Effect Transistors," September 1965.

23. Leppala, R., "A Maximum Power Transfer Device for Use With Solar Cell," September 1965.

24. Pakos, Paul E., "A Voltage Squaring Circuit and Analog to Digital Converter for Pulsed Systems," June 1965.

25. Walker, William G., "A High-Power One-Millisecond Pulse-Forming Network," June 1965.

26. Tobey, M., "Noise Measurements of Thin Cadmium Sulfide Films," June 1964.

27. Roberge, James K., "Design of Spacecraft Radar Systems for Investigation of the Planet Venus," June 1962.

28. Zimmerman, D., "A Low-Power Noise Source for Dicke Radiometer," (in progress).

Bachelor of Science

29. Adams, J., "Triggering Series-Connected Silicon Controlled Rectifiers," June 1965.

30. Ebner, G., "Capacitive Properties of the Cadmium Sulfide Thin Film Diode," May 1964.

31. Fulton, D., "The Construction and Evaluation of Cadmium Sulfide Thin Film Transistors," May 1964.

32. Lappin M., "Energy Distribution of Trapping Centers in Thin Film Cadmium Sulfide," May 1964.

33. Warakomsky, R., "A Regulated Power Supply for Spacecraft Use," May 1964.

VIII PARTICIPANTS IN THE PROJECT

FACULTY

Professor J. F. Reintjes, Principal Investigator
Professor J. G. Gottling

STAFF MEMBERS

J. A. Bosco
L. W. Counts
J. R. Sandison

RESEARCH ASSISTANTS

E. L. Arnn
A. A. Aponick
R. K. Breon
R. M. Cornew
M. L. Dertouzos
M. Osman
J, K. Roberge
W. G. Sadler
J. H. Taylor
D. E. Zimmerman

THESES STUDENTS AND STUDENT EMPLOYEES

J. Adams
R. C. Buelte
D. R. Cobb
G. C. Ebner
J. Edgerton
D. E. Fulton
M. G. Lappin
R. A. Leppala
P. E. Pakos
P. B. Robb
M. C. Tobey
W. G. Walker
R. E. Warakomsky

APPENDIX A

SYNTHETIC APERTURE RADARS

Although the main thrust of the project was on the development of a simple, conventional, pulse-radar-type instrument for making backscatter measurements, some attention was given to the use of synthetic-aperture radars for the construction of radar images of planetary surfaces. Imaging radars are attractive for planetary-surface investigations because they provide a radar map of the surfaces illuminated. The over-all system requires more elaborate equipment, however, since the r-f radiation must be coherent, storage of signal returns must be included, and a means must be provided for processing the raw data in the returned signal into an interpretable picture. When measurements are made from a spacecraft, signal processing is most easily conducted at an earth-based station.

An important factor is the design of synthetic-aperture surface-mapping radars that operate in satellites, and spacecraft is the choice of the transmitter waveform. Related to this parameter are the range from satellite to surface and ambiguities in Doppler signals that may arise. With a pulsed radar, the radar pulse repetition frequency (prf) must be set at a value which is at least twice the highest Doppler-frequency component that is present within the antenna azimuth beamwidth. For this prf, range ambiguities can occur under certain conditions of range.

Consider the diagrams shown in Fig. A-1. The objective is to select a prf high enough to sample the highest Doppler frequency present in the main beam of the antenna (this avoids azimuth ambiguities), and then to limit the extent of the surface swath g so that no range ambiguities can occur. This procedure must be followed since it is possible for the two-range delay time $\left(\frac{2r_2}{c}\right)$ to be greater than the radar interpulse period required for Doppler-frequency sampling.

If only a narrow surface swath is to be covered, the range will be unambiguous if the slant range difference $r_2 - r_1$ is less than $\frac{cT}{2}$, where T is the interpulse period and c is the velocity of light. It is assumed here that antenna side lobes produce no discernible signal returns, a reasonable assumption if the angle θ is small.

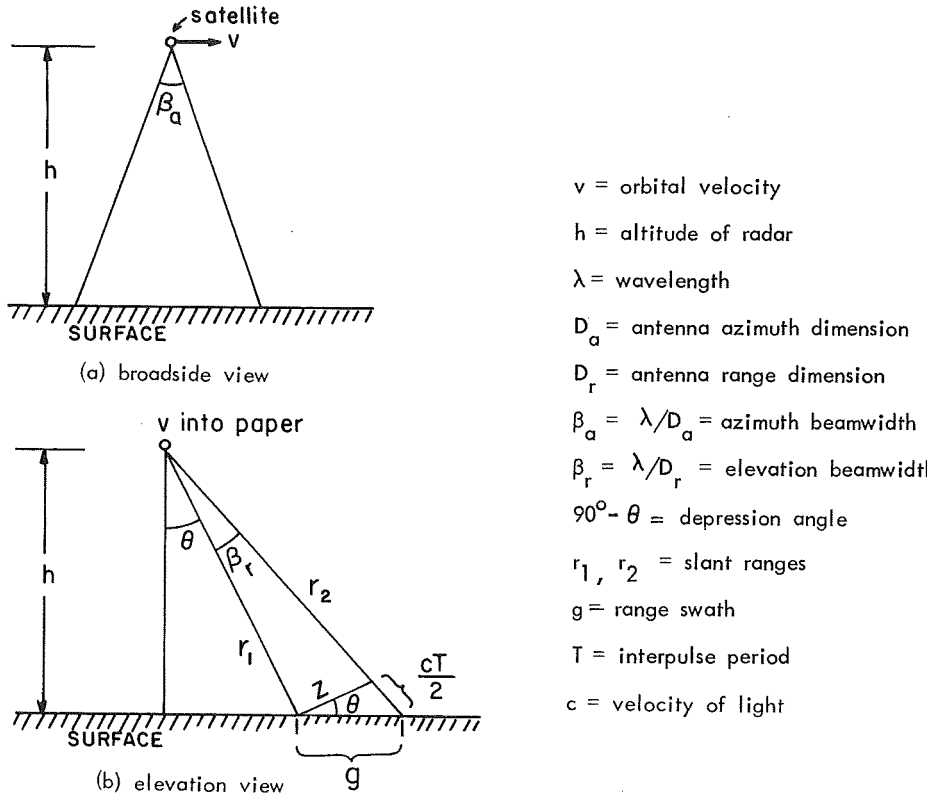

Fig. A-1 Diagrams for the Calculation of Range and Doppler Ambiguities

The calculations presented below are based on a flat surface; they are intended to show the interrelation among parameters such as antenna size, prf, resolution and surface coverage. The Doppler shift f_d at the beam edge, where maximum shift occurs, is

$$f_d = \frac{2v}{\lambda} \sin(\beta_a/2) \qquad \text{(A-1)}$$

For small values of β_a,

$$f_d \doteq \left(\frac{2v}{\lambda}\right)(\beta_a/2) \qquad \text{(A-2)}$$

Substituting for β_a its value λ/D_a gives for f_d the relationship

$$f_d \doteq \left(\frac{v}{\lambda}\right)\left(\frac{\lambda}{D_a}\right) = \frac{v}{D_a}$$

The sampling frequency for f_d should be at least $2f_d$. Hence,

$$prf = 2f_d = \frac{2v}{D_a} = \frac{1}{T} \qquad \text{(A-3)}$$

It should be noted that the sampling frequency $1/T = 2v/D_a$ is based on an antenna azimuth beam angle $\beta_a = \lambda/D_a$. In practice, with an aperture of dimension D_a, it is not possible to obtain a beam of width λ/D_a and also negligible side lobes. A "safety factor" in the form of a smaller dimension for D_a should therefore be introduced. If non-uniform response within the main beam is ignored, it is possible to achieve negligible side lobes outside a beam angle that has a value of approximately $\sqrt{2}\lambda/D_a$. Thus, in practice, the prf may be expressed as

$$prf = \frac{2\sqrt{2}\,v}{D_a} = \frac{1}{T} \qquad \text{(A-4)}$$

From Fig. A-1b, assuming a value for $\beta_r = \sqrt{2}\,\lambda/D_r$, we obtain

$$z \doteq r_1 \tan\beta_r = \left(\frac{h}{\cos\theta}\right)\left(\tan\beta_r\right)$$

For small values of β_r, $\tan\beta_r \doteq \beta_r$. Hence,

$$z \doteq \left(\frac{h}{\cos\theta}\right)\left(\frac{\sqrt{2}\,\lambda}{D_r}\right)$$

Therefore,

$$g = \frac{z}{\cos\theta} \doteq \frac{\sqrt{2}h\,\lambda}{D_r \cos^2\theta} \qquad \text{(A-5)}$$

From the geometry of Fig. A-1b the surface swath g outside of which returns may be assumed negligible is

$$g = \frac{cT}{2\sin\theta} \qquad \text{(A-6)}$$

However, for good mapping the surface swath should be assumed somewhat narrower, say $g/\sqrt{2}$; thus, when this range safety factor is included,

$$g = \frac{cT}{2\sqrt{2}\sin\theta} \tag{A-7}$$

and from Eq. A-5

$$g \doteq \frac{h\lambda}{D_r \cos^2\theta} \tag{A-8}$$

Combining Eqs. A-7 and A-8, yields

$$\frac{h\lambda}{D_r \cos^2\theta} = \frac{cT}{2\sqrt{2}\sin\theta}$$

Solving for D_r gives

$$D_r = \frac{2\sqrt{2}\, h\lambda \sin\theta}{cT\cos^2\theta} \tag{A-9}$$

Substituting Eq. A-4 into Eq. A-9 yields

$$D_r D_a = \frac{8\, h\lambda v \sin\theta}{c\cos^2\theta} = 8\, r_1 \lambda \frac{v}{c}\tan\theta \tag{A-10}$$

We can now make the following observations:

(a) The maximum available azimuth resolution (based on the time available for observation with a fixed antenna) is equal to one-half the antenna azimuth dimension $D_a/2$ and the slant-range resolution is dependent upon pulse width. The surface-range resolution is degraded from slant-range resolution by a factor $\csc\theta$, which is large for small values of θ.

(b) The interpulse period T must be adjusted to accommodate division of the $D_r D_a$ product between its two factors D_r and D_a.

(c) Surface-swath coverage g is determined by D_r, h, λ and θ.

(d) As angle θ increases, the surface-range coverage decreases but the surface-range resolution becomes finer and tends toward the slant-range resolution.

(e) A relaxed requirement on azimuth resolution is not generally useful for easing antenna-design requirements but does allow a greater range swath to be mapped.

Let us now consider a numerical example. Suppose a radar with a synthetic-aperture antenna is installed in a satellite flying at an altitude h = 1000 kilometers above a planetary surface. Assume the satellite velocity $\underline{v}$ is 7,200 meters per second, and choose a radar wavelength $\lambda = 0.3$ meter. Let the antenna depression angle be 60°; that is, $\theta = 15^{\circ}$. From Eq. A-10

$$D_r \cdot D_a = \frac{(8)\ (10^6)\ (0.3)\ (7.2 \times 10^3)\ (0.26)}{(3 \times 10^8)\ (0.94)} = 16 \text{ meters}^2$$

Choose $D_a = D_r = 4$ meters. From Eq. A-4

$$\text{prf} = \frac{(2\sqrt{2})\ (7.2 \times 10^3)}{4} = 5.1 \text{ kHz}$$

From Eq. A-7

$$g = \frac{(3 \times 10^8)\ (0.196 \times 10^{-3})}{(2\sqrt{2})\ (0.26)} = 80 \text{ kilometers} = 50 \text{ miles}$$

Thus the radar will map a surface swath 50 miles wide. The surface-range resolution within the swath is determined by the pulse duration; for a 0.1-microsecond pulse, since 0.1μ sec pulse equivalent to a 50-ft. slant-range resolution, the surface-range resolution will be (50 x csc 15°) = 197 feet. Azimuth resolution can be as fine as 2 meters (6.6 ft) — the resolution obtainable if the entire train of echoes returned by a simple scatterer during the passage of the antenna beam is utilized in synthetic-aperture processing.

It may be noted that the choice of parameters in the example yields a possible azimuth resolution much finer than the range resolution. Surface-range resolution degrades rapidly as θ approaches zero degrees. It can be improved by transmitting a frequency-modulated (chirp) pulse of large bandwidth; the received echoes are concentrated in the receiver into pulses of width equal to the reciprocal of the frequency-modulation bandwidth. However, a synthetic-

aperture radar using wide-band chirp to provide fine resolution in both range and azimuth (say, of the order of 7 ft. in each direction) generates such a tremendous quantity of map data that difficulty may be encountered in storing all the data on board and transmitting it to an earth station. A more practical possibility may therefore be a simpler system that processes only a fraction of the echoes received from each scatterer so as to achieve an azimuth resolution equal to an easily obtained range resolution — say, a few hundred feet in each direction.